

Numerical Investigation of Observational Flux Partitioning Methods for Water Vapor and Carbon Dioxide

Einara Zahn¹, Khaled Ghannam^{2,3}, Marcelo Chamecki⁴, Arnold F. Moene⁵,
William P. Kustas⁶, Stephen Good⁷, Elie Bou-Zeid¹

¹Department of Civil and Environmental Engineering, Princeton University, Princeton, New Jersey, USA

²Program in Atmospheric and Oceanic Sciences (Cooperative Institute for Modeling the Earth System),
Princeton University, Princeton NJ, USA

³Department of Civil and Environmental Engineering, Northeastern University, Boston, MA

⁴Department of Atmospheric & Oceanic Sciences, University of California in Los Angeles, Los Angeles,
California, USA

⁵Meteorology and Air Quality Group, Wageningen University and Research, Wageningen, The
Netherlands

⁶USDA-ARS, Hydrology and Remote Sensing Lab, Beltsville, MD 20705-2350, USA

⁷Department of Biological and Ecological Engineering, Oregon State University, Corvallis, OR 97331,
USA

Key Points:

- The performance of four partitioning methods are explored with aid of Large Eddy Simulations
- The method's performance are shown to depend on flux ratios, canopy sparseness, and measurement height
- The correlation coefficient between CO₂ and water vapor is shown to help inform the choice of water-use efficiency models

Corresponding author: Elie Bou-Zeid, ebouzeid@princeton.edu

Abstract

While yearly budgets of CO₂ and evapotranspiration (ET) above forests can be readily obtained from eddy-covariance measurements, the quantification of their respective soil (respiration and evaporation) and canopy (photosynthesis and transpiration) components remains an elusive yet critical research objective. To this end, methods capable of reliably partitioning the measured ET and F_c fluxes into their respective soil and plant sources and sinks are highly valuable. In this work, we investigate four partitioning methods (two new, and two existing) that are based on analysis of conventional high frequency eddy-covariance (EC) data. The physical validity of the assumptions of all four methods, as well as their performance under different scenarios, are tested with the aid of large eddy simulations, which are used to replicate eddy-covariance field experiments. Our results indicate that canopies with large, exposed soil patches increase the mixing and correlation of scalars; this negatively impacts the performance of the partitioning methods, all of which require some degree of uncorrelatedness between CO₂ and water vapor. In addition, best performance for all partitioning methods were found when all four flux components are non-negligible, and measurements are collected close to the canopy top. Methods relying on the water-use efficiency (W) perform better when W is known a priori, but are shown to be very sensitive to uncertainties in this input variable especially when canopy fluxes dominate. We conclude by showing how the correlation coefficient between CO₂ and water vapor can be used to infer the reliability of different W parameterizations.

Plain Language Summary

Forests and vegetated ecosystems play a crucial role in the exchange of CO₂ and water vapor with the atmosphere. During the day, plants absorb CO₂ through photosynthesis (P), releasing water vapor via transpiration (T). On the other hand, the forest floor contributes to CO₂ through respiration (R), and moist soil leads to water vapor evaporation (E). While tall towers currently measure total CO₂ ($F_c = P + R$) and water vapor ($ET = E + T$) exchanges, distinguishing the contributions from soil respiration and evaporation versus tree photosynthesis and transpiration remains a challenge. This study addresses this gap by investigating methods to separate F_c and ET into their individual components. Using a simulated forest environment with a virtual meteorological tower, the study tests four methods to estimate respiration, photosynthesis, evaporation, and transpiration. Results reveal that more reliable estimates are obtained when measurements are collected close to the forest top, especially without significant vegetation gaps leading to strong mixing. Additionally, the study highlights the expected errors in two approaches when faced with real-world uncertainties. By elucidating optimal conditions for method application, this research contributes to advancing our understanding of ecosystem-atmosphere interactions and informs the accurate measurement of vital components in the carbon and water cycles.

1 Introduction

Land-atmosphere exchanges of water vapor and CO₂ are important components of the global water and carbon cycles. In this context, vegetated canopies, such as forests, play an important role in both cycles through their contributions to evapotranspiration (ET) and net CO₂ exchange (F_c). Facilitated by an extensive network of eddy-covariance (EC) towers setup across the globe, we are currently able to quantify the long-term budgets for both quantities over many land use types. Nonetheless, long-term quantification of their individual soil (evaporation and respiration) and plant canopy (transpiration and photosynthesis) components is an equally important but much more challenging research goal. While different methods have been proposed to measure one or more of these components, such as soil chambers, sap-flow and leaf-level measurements, they are still un-

able to offer unified long-term measurements (yearly scale) of all components across different ecosystems. This poses a challenge to understanding, for instance, how different environmental, meteorological, and climatological conditions affect these processes, which are urgent research questions as we attempt to mitigate and adapt to climate change and variability (Mengis et al., 2015; Kirschbaum & McMillan, 2018; Dusenke et al., 2019; Baslam et al., 2020; Wang et al., 2022). Therefore, the development and implementation of practical and accurate methods to partition the total ET and F_c fluxes that are currently being measured world-wide is a significant objective, particularly if such methods can solely rely on eddy-covariance data.

Several methods have been proposed in the last decade to partition the total ET and F_c . In terms of CO_2 components, one of the most popular approaches consists of modeling soil respiration (R_{soil}) based on a soil temperature response function (Reichstein et al., 2005; Lasslop et al., 2010), thus obtaining gross-primary productivity (GPP) as $GPP = F_c - R_{soil}$. The conceptual framework behind each of the various available partitioning algorithms for ET varies widely. For instance, after reviewing ET partitioning results from several sites, Wei et al. (2017) proposed a formulation linking T/ET to the leaf-area index (LAI). Perez-Priego et al. (2018) and X. Li et al. (2019), on the other hand, adopted a physiological approach; the authors use a big-leaf scheme to first model and later relate plant conductance to transpiration. Other authors explored the direct connection between plant photosynthesis and transpiration — through the ecosystem water-use efficiency ($eW = GPP/ET$) — to derive empirical formulations based on the correlation between these components (Zhou et al., 2016; Scott & Biederman, 2017). In addition, machine learning algorithms have also been used (Nelson et al., 2018; Rigden et al., 2018; Eichelmann et al., 2022) to link T or E to environmental variables. While these approaches have gained attention and multi-comparison studies have become more popular (Nelson et al., 2020), they usually invoke uncertain models for individual components or require additional (and hard to measure) environmental variables, precluding their wider implementation. For instance, most of these methods require GPP as an input in order to partition ET , thus increasing the uncertainties in their outputs. Therefore, approaches able to simultaneously partition CO_2 and ET , based solely on available EC data, offer many advantages over the previously mentioned methods.

A particularly useful class of partitioning methods, that this paper focuses on, are approaches based on turbulent statistics computed from high-frequency data. Not only do they require few (usually only water use efficiency) or no extra inputs, but they also allow the simultaneous and consistent partitioning of ET and F_c flux components. Three previously proposed methods are the flux-variance similarity (FVS) (Scanlon & Sahu, 2008; Scanlon & Kustas, 2010; Scanlon et al., 2019), the modified relaxed-eddy accumulation (MREA) (C. Thomas et al., 2008), and the conditional eddy covariance (CEC) (Zahn et al., 2022).

Zahn et al. (2022) intercompared FVS, MREA and CEC across four experimental sites, including a grass site with independent estimates of transpiration and a forest site with soil respiration measurements. While reasonable results were obtained in different situations for all three approaches, a general conclusion regarding their broad applicability across different ecosystems was not attained. Part of the challenge is related to the difficulty in validating the methods' formulation and results. In addition, validating their universality — *i.e.*, when and where they perform well — would require tower data across a wide range of ecosystem types and climatic conditions that could result in various combinations of flux component strengths.

Previously, Klosterhalfen, Moene, et al. (2019) used LES to investigate the physical assumptions and the performance of the FVS method. The authors showed that FVS is very sensitive to one of the assumptions invoked during its derivation, a necessary algebraic manipulation to obtain a closed system of equations. FVS was also found to be very sensitive to the plant water-use efficiency (W), which is the only input to the model

that is not directly computed from the time series. Thus, the main disadvantage of the FVS method is that it presumes that a very important piece of information, W , is already known. However, the challenge remains that while different alternatives to parameterize W are available (Skaggs et al., 2018; Scanlon et al., 2019), the different options usually do not match and are shown to result in different flux partitioning outputs (Wagle et al., 2021). In addition, many studies (Sulman et al., 2016; Klosterhalfen, Graf, et al., 2019; Wagle et al., 2021; Zahn et al., 2022) have shown that, depending on the site, the rate of valid solutions found by the FVS method can be as low as 30%.

To overcome limitations of field experiments in answering many of the open research questions, in this study we use numerical simulations of canopy flows relying on the Large-Eddy Simulations (LES) (Stoll et al., 2020) technique with embedded virtual flux towers and sensors. One of the biggest advantages LES offers in the present study is that the true flux components and water-use efficiency are known inputs; therefore, the results for the implemented partitioning methods, which are applied to time series sampled during the simulation, can be validated. We thus further investigate the advantages and limitations of FVS, MREA, and CEC. In contrast to the FVS method, the formulation of which starts from the similarity equations for variances but then invokes empirical assumptions, both CEC and MREA are fully empirical approaches based on the assumption that CO_2 and H_2O are similarly transported by turbulence from their shared soil and canopy sinks and sources. While their formulation cannot be rigorously proven, their assumptions and performance can be extensively tested in LES under various conditions.

Cognizant of potential limitations of FVS, CEC, and MREA, in the present study we also formulate and test two related approaches. The first approach is the conditional eddy accumulation or CEA, which complements the other tested methods better. The Conditional Eddy Accumulation method combines quadrant analyses and the traditional Relaxed Eddy Accumulation method (Businger & Oncley, 1990). While it uses similar principles as adopted by the Modified Relaxed Accumulation method (see C. Thomas et al. (2008) and Zahn et al. (2022)) and CEC, CEA's formulation also includes down-drafts in its framework, and yields different results. The second method is a hybrid approach that assimilates W into the CEC method, and is here called CECw. The idea behind CECw is to investigate how much skill the water-use efficiency alone adds to partitioning.

An important question with these multiple available approaches is under what conditions (measurement height, season, canopy characteristics, etc.) are some approaches more accurate than others. As discussed by Zahn et al. (2022), the assumption that eddies from the soil can be distinguished from those coming from the plant canopy would suggest that more realistic results should be obtained for both methods over sparser canopies (a conclusion we will revisit here). The authors also concluded that the high-frequency data should be measured as close as possible to the canopy so as to sample the transporting eddies before turbulence mixes canopy and soil fluxes. One question that remains open is whether sparser canopies allow a higher measurement height given the stronger horizontal distinction between canopy and soil. The importance of plant canopy "openness" is thus investigated in the present simulations. To that end, we first simulate flow over a homogeneous canopy, where the canopy presence (*i.e.*, fluxes and drag) is felt at every grid point of the lower part of the domain; to simulate canopy sparseness, we then include exposed patches of soil resembling crop organizations such as vineyards. Another related key question is how (not if) the methods' performances are affected by the relative magnitude of soil versus canopy fluxes. To address that question, we investigate a broad range of combinations of the ratios of photosynthesis/respiration and transpiration/evaporation, and how they influence the outcome of each method.

Overall, this paper explores how similarity-based partitioning approaches perform under various conditions encountered in real field experiments, and how simple turbu-

lence measurements can help understand the biophysiological behavior of plant canopies. The following questions are investigated

1. How does the sparseness of the canopy impact the assumptions of the methods and their performance?
2. How does the magnitude of the individual four flux components influence partitioning skill?
3. What is the role of the measurement height for different levels of canopy sparseness?
4. How sensitive are the FVS and CECw methods to errors in water use efficiency?

The answers to these questions will further deepen our understanding of ET and F_c partitioning and the reliability of the investigated methods. They will also help to broadly identify the best practices for future experimental campaigns aimed at obtaining flux component estimates.

2 Theory

We start this section with a brief summary of the partitioning methods investigated, where the main equations and necessary inputs are discussed. Throughout the text, the concentrations of CO_2 and H_2O are defined as c and q , respectively. The velocity components in the streamwise (x), cross-stream (y), and vertical directions (z) are u , v , and w , while the deviation of a variable μ around its time and/or space average $\bar{\mu}$ is denoted using a prime $\mu' = \mu - \bar{\mu}$. An important note to make here is that, for the remainder of the paper, we will not distinguish between soil and plant respiration. All the tested methods cannot make this distinction either since they are interrogating the properties of air parcels coming from the plants with the lumped information about gross primary production (GPP), and thus they partition net ecosystem exchange into GPP and R_{soil} . In our LES setup and the rest of the paper, however, CO_2 will be emitted from the soil only, and we will refer to it as R , while the simulated plants only assimilate CO_2 , and we refer to that flux as photosynthesis (P).

2.1 Brief description of the partitioning methods

In what follows, a summary of the FVS, CEC, and the newly proposed CEA and CECw, is presented. We note that results for the MREA method, previously explored in Zahn et al. (2022), were almost identical to CEC and thus will not be reported in this paper.

2.1.1 Flux-variance similarity (FVS) method

The flux-variance similarity method combines the similarity equations for variances of c and q with the water-use efficiency $W = P/T$ (Scanlon & Sahu, 2008; Scanlon & Kustas, 2010). More specifically, it rewrites the budgets by separating the two scalars into their soil (c_r for respiration and q_e for evaporation) and canopy (c_p for photosynthesis and q_t for transpiration) components. To close the system of equations, the following approximations are needed (G. Katul et al., 1995)

$$\rho_{c_p, c_r} \approx \frac{\rho_{w, c_r}}{\rho_{w, c_p}} \quad \text{and} \quad \rho_{q_t, q_e} \approx \frac{\rho_{w, q_e}}{\rho_{w, q_t}}, \quad (1)$$

where ρ_{xy} is the correlation coefficient between the variables x and y . After some algebra, the final equations for the ratios of flux components are

$$\frac{E_{FVS}}{T_{FVS}} = -\rho_{c_p, c_r}^2 + \rho_{c_p, c_r}^2 \sqrt{1 - \rho_{c_p, c_r}^{-2} \left(1 - W^2 \sigma_q^2 / \sigma_{c_p}^2\right)}, \quad (2a)$$

$$\frac{R_{FVS}}{P_{FVS}} = -\rho_{c_p, c_r}^2 \pm \rho_{c_p, c_r}^2 \sqrt{1 - \rho_{c_p, c_r}^{-2} \left(1 - \sigma_c^2 / \sigma_{c_p}^2\right)}, \quad (2b)$$

where ρ_{c_p, c_r} and σ_{c_p} , the standard deviation of c_p , are directly computed by the two following complementary equations (Skaggs et al., 2018; Scanlon et al., 2019),

$$\sigma_{c_p}^2 = \frac{(1 - \rho_{c,q}^2) (\sigma_q \sigma_c W)^2 \left(\sigma_q^2 w' c'^2 - 2 \rho_{c,q} \sigma_q \sigma_c \overline{w' c'} \overline{w' q'} + \sigma_c^2 \overline{w' q'}^2 \right)}{\left[\sigma_c^2 \overline{w' q'}^2 + \sigma_q^2 \overline{w' c'} W - \rho_{c,q} \sigma_q \sigma_c (\overline{w' c'} + \overline{w' q'} W) \right]^2}, \quad (3)$$

$$\rho_{c_p, c_r}^2 = \frac{(1 - \rho_{c,q}^2) \sigma_q^2 \sigma_c^2 (\overline{w' c'} - \overline{w' q'} W)^2}{\left(\sigma_q^2 \overline{w' c'}^2 - 2 \rho_{c,q} \sigma_q \sigma_c \overline{w' q'} \overline{w' c'} + \sigma_c^2 \overline{w' q'}^2 \right) (\sigma_c^2 - 2 \rho_{c,q} \sigma_q \sigma_c W + \sigma_q^2 W^2)}. \quad (4)$$

The standard deviation of c , σ_c , and q , σ_q , and the correlation coefficient between c and q , $\rho_{c,q}$, are also needed and can be directly computed from the measured time series. The water-use efficiency — which is an input to the method — must be separately measured or estimated (a description of how to parameterize W can be found elsewhere (Scanlon & Kustas, 2010; Skaggs et al., 2018; Zahn et al., 2022)). For our numerical simulations, W is a known input. However, even the correct water-use efficiency will only result in realistic solutions if the following conditions are met (Scanlon et al., 2019)

$$\rho_{c,q}^{-1} \frac{\sigma_c}{\sigma_q} \leq \frac{\overline{w' c'}}{\overline{w' q'}} < \rho_{c,q} \frac{\sigma_c}{\sigma_q} \quad \text{for } \rho_{c,q} < 0, \text{ and} \quad (5a)$$

$$\frac{\overline{w' c'}}{\overline{w' q'}} < \rho_{c,q} \frac{\sigma_c}{\sigma_q} \quad \text{for } \rho_{c,q} > 0. \quad (5b)$$

Failure to satisfy the above expressions has been shown to be the main cause of low availability of physically valid solutions across sites (Wagle et al., 2021; Zahn et al., 2022).

2.1.2 Conditional eddy covariance (CEC) method

The conditional eddy covariance method (Zahn et al., 2022) expands the MREA framework proposed by C. Thomas et al. (2008). Similarly to MREA, CEC conditionally samples ejections originating from the soil that are rich in CO_2 and H_2O ($w' > 0$, $c' > 0$, and $q' > 0$); in addition, it also samples ejections that were in contact with the canopy and are depleted in CO_2 and rich in water vapor ($w' > 0$, $c' < 0$, and $q' > 0$), which is not done in the MREA framework. The data points of a time series of length N that are identified to be in contact with soil or canopy are then used to compute “sample” fluxes of evaporation (f_E) and respiration (f_R) or transpiration (f_T) and photosynthesis (f_P) (see Figure 1 in Zahn et al. (2022)). These sample fluxes are given by the following expressions

$$f_E = \frac{1}{N} \sum I_S w' q' \quad \text{and} \quad f_R = \frac{1}{N} \sum I_S w' c' \quad (6)$$

$$f_T = \frac{1}{N} \sum I_C w' q' \quad \text{and} \quad f_P = \frac{1}{N} \sum I_C w' c', \quad (7)$$

where I_S is an indicator function that selects only “soil surface eddies”, *i.e.*, data points that satisfy $c' > 0$, $q' > 0$, $w' > 0$; I_C , on the other hand, selects only eddies that were in touch with the canopy where we expect $c' < 0$, $q' > 0$, $w' > 0$. Sample fluxes were only computed when the respective quadrant contained at least 2% of the data points. If, on the other hand, $\sum I_S / N < 2\%$ (or $\sum I_C / N < 2\%$), we attribute all fluxes to canopy (or soil) components.

The expressions given in (6) and (7) are not the actual fluxes of each component; instead, they are assumed to be “sample” indicative fluxes that we can use to estimate the ratio of the total fluxes by the following:

$$r_{ET} = \frac{f_E}{f_T} = \frac{E_{CEC}}{T_{CEC}} \quad \text{and} \quad r_{RP} = \frac{f_R}{f_P} = \frac{R_{CEC}}{P_{CEC}}. \quad (8)$$

The separate flux components are then obtained by combining the flux ratios with the expressions for total fluxes ($ET = T + E$ and $F_c = R + P$). However, as discussed by Zahn et al. (2022), a mathematical constraint (division by zero) happens whenever $\frac{R_{CEC}}{P_{CEC}} \approx -1$, but affects only the partitioning for CO_2 flux components. Because the FVS method also computes the flux ratios, the same mathematical constraint arises when $\frac{R_{FVS}}{P_{FVS}} \approx -1$. Therefore, solutions in this limit must be carefully inspected (and removed) for both methods.

2.1.3 Conditional Eddy Accumulation (CEA) method

The traditional Relaxed Eddy Accumulation method (Businger & Oncley, 1990) was derived as an alternative to eddy-covariance measurements for scalars s that cannot be measured at a high frequency. The method consists of separately measuring the average scalar concentrations associated with updrafts (\bar{s}^+) and concentrations associated with downdrafts (\bar{s}^-), estimating the total scalar flux (F_s) as

$$F_s = \beta \sigma_w (\bar{s}^+ - \bar{s}^-), \quad (9)$$

where σ_w is the standard deviation of the vertical velocity and β is a constant.

By taking into account only updrafts rich in CO_2 and H_2O , C. Thomas et al. (2008) modified equation (9) and proposed the MREA method. The CEA method, on the other hand, retains the information from downdrafts and estimates an analogue to \bar{s}^+ and \bar{s}^- for each individual flux component. In the framework proposed here, we compute \bar{c}_r^+ and \bar{q}_e^+ (using $c' > 0$, $q' > 0$, $w' > 0$) and \bar{c}_r^- and \bar{q}_e^- ($c' < 0$, $q' < 0$, $w' < 0$), both representing respiration and evaporation (note that the fluxes in both cases are positive). For canopy components, we compute \bar{c}_p^+ and \bar{q}_t^+ ($c' < 0$, $q' > 0$, $w' > 0$) and \bar{c}_p^- and \bar{q}_t^- ($c' > 0$, $q' < 0$, $w' < 0$), where the fluxes are now negative for c (photosynthesis) and positive for q (transpiration). These conditional averages are computed as

$$\bar{c}_r^+ = \frac{1}{N_S^+} \sum c' I_S^+ \quad \text{and} \quad \bar{q}_e^+ = \frac{1}{N_S^+} \sum q' I_S^+, \quad (10)$$

$$\bar{c}_r^- = \frac{1}{N_S^-} \sum c' I_S^- \quad \text{and} \quad \bar{q}_e^- = \frac{1}{N_S^-} \sum q' I_S^-, \quad (11)$$

$$\bar{c}_p^+ = \frac{1}{N_C^+} \sum c' I_C^+ \quad \text{and} \quad \bar{q}_t^+ = \frac{1}{N_C^+} \sum q' I_C^+, \quad (12)$$

$$\bar{c}_p^- = \frac{1}{N_C^-} \sum c' I_C^- \quad \text{and} \quad \bar{q}_t^- = \frac{1}{N_C^-} \sum q' I_C^-, \quad (13)$$

where N and I are the number of sampled events and the indicator functions defined according to the origin of fluxes (subscript ‘S’ for soil and ‘C’ for canopy) separated by updrafts (+) and downdrafts (-).

By assuming that the coefficient β is constant or weakly dependent on stability (Businger & Oncley, 1990; G. G. Katul et al., 1996; Zahn et al., 2023), and that σ_w is the same regardless of conditional sampling, we approximate the flux ratios as

$$r_{ET} = \frac{E_{CEA}}{T_{CEA}} = \frac{\bar{q}_e^+ - \bar{q}_e^-}{\bar{q}_t^+ - \bar{q}_t^-}, \quad (14)$$

$$r_{RP} = \frac{R_{CEA}}{P_{CEA}} = \frac{\bar{c}_r^+ - \bar{c}_r^-}{\bar{c}_p^+ - \bar{c}_p^-}. \quad (15)$$

306 A diagram illustrating the method is shown in Figure 1, where we show points clas-
 307 sified following the conditional sampling, as well as the average values as defined in (10)–
 308 (13). When plant components dominate the fluxes (E and R), we expect the denomi-
 309 nator in (14) and (15) to be larger, as indicated in plot 1a and b; however, for fluxes dom-
 310 inated by soil components, the numerators are larger (plot 1c and 1d).

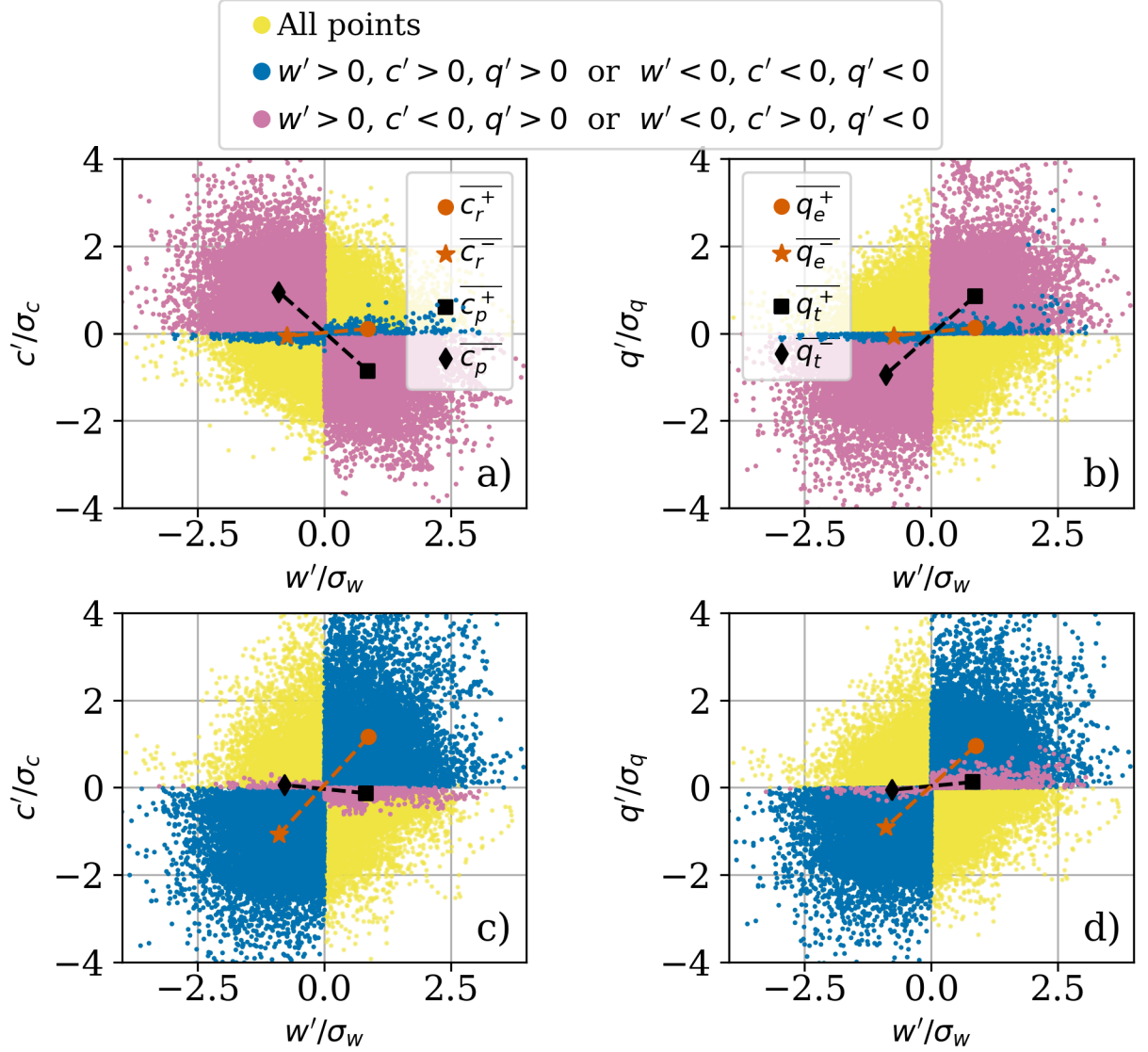


Figure 1. Quadrant plots illustrating the Conditional Eddy Accumulation (CEA) method, where the points selected to compute ratios in Eqs. (14) (plots a and c) and (15) (plots b and d) are shown. Figure generated using time series from large-eddy simulations. Plots a) and b) have ratios $T/E=|P|/R=5$, while plots c) and d) have ratios $T/E=|P|/R=0.2$.

311 2.1.4 Combining CEC and water use efficiency

312 Both CEC and CEA have the practical advantage of not requiring *a priori* knowl-
 313 edge of the water use efficiency. However, if W is known, it can in fact inform both meth-
 314 ods. Therefore, we now combine the flux ratios as defined by the CEC method with the

water-use efficiency and derive an alternative partitioning method that we will refer to as CECw. The goal of this new model is to investigate if, given the correct water-use efficiency, a simpler method could perform similarly to the FVS method, potentially being easier to implement and yielding solutions more often. This ultimately will indicate how important W is to the skill of the FVS method.

We start the derivation by combining the water-use efficiency ($W = P/T$) and the flux ratios as defined by CEC ($r_{RP} = R/P$ and $r_{ET} = E/T$),

$$W = \frac{P}{T} = \frac{R}{E} \frac{r_{ET}}{r_{RP}} = Z \frac{r_{ET}}{r_{RP}}, \quad (16)$$

where we define $Z = R/E$.

Rewriting the equations for total fluxes and introducing the definitions of W and Z , we have

$$F_c = W \times T + R, \quad (17)$$

$$T = ET - \frac{R}{Z}. \quad (18)$$

Combining equations (17) and (18) and rewriting for R , we get the following expression for soil respiration

$$R_{\text{CECw}} = \frac{F_c - W \times ET}{1 - \frac{W}{Z}} = \frac{F_c - W \times ET}{1 - \frac{r_{ET}}{r_{RP}}}, \quad (19)$$

where the ratios r_{RP} and r_{ET} are computed from equations (6)–(8). Similarly, we can obtain an expression for T_{CECw}

$$T_{\text{CECw}} = \frac{F_c - W \times ET \times \frac{r_{RP}}{r_{ET}}}{1 - \frac{r_{RP}}{r_{ET}}}. \quad (20)$$

Corresponding expressions can be derived for P_{CECw} and E_{CECw} , or they can then be computed as the residuals of the total eddy-covariance (EC) fluxes (both approaches yield identical results since the total flux expression are directly used in the derivation). Because $r_{ET} > 0$ and $r_{RP} < 0$, this equation has no mathematical singularity. Nonetheless, under certain conditions the method can result in negative transpiration or respiration. Therefore, we must also ensure that $T_{\text{CECw}} > 0$ and $R_{\text{CECw}} > 0$. In addition, we also tested the method by computing the ratios following the CEA method (expressions (14) and (15)), but the results for CECw were similar and thus not included here.

3 Methods

This section describes the setup of our numerical simulations and how the time series were sampled and processed for partitioning.

3.1 Large-eddy simulations

The LES algorithm used in this study has been extensively tested over homogeneous and heterogeneous surfaces, with and without resolved roughness elements (Bou-Zeid et al., 2005; Kumar et al., 2006; Q. Li & Bou-Zeid, 2019; Huang & Bou-Zeid, 2013; Zahn & Bou-Zeid, 2023). Its formulation is based on the solution of the spatially filtered incompressible continuity (equation (21)) and Navier-Stokes (equation (22)) equations under the Boussinesq approximation. The conservation equation for a scalar s (equation (23)) is also solved for c_r , c_p , q_e , and q_t . Since only neutral conditions are considered, the effects of buoyancy are ignored in our analyses. To ensure that our canopy flow simulations, covering $\approx 14\%$ of the ABL (1km) height, closely represent the turbulent

profiles expected when the full ABL is simulated, we followed the recommendations from Zahn and Bou-Zeid (2023). In this setup, in addition to a large-scale pressure term, the force balance also includes a stress at the top of the domain in addition to the Coriolis term. More details are given below and discussed in Zahn and Bou-Zeid (2023).

$$\frac{\partial \tilde{u}_i}{\partial x_i} = 0, \quad (21)$$

$$\frac{\partial \tilde{u}_i}{\partial t} + \tilde{u}_j \left(\frac{\partial \tilde{u}_i}{\partial x_j} - \frac{\partial \tilde{u}_j}{\partial x_i} \right) = - \frac{\partial p^*}{\partial x_i} - \frac{\partial \tau_{ij}}{\partial x_j} + f_c \epsilon_{ij3} (\tilde{u}_j - u_j^G) + D_i, \quad (22)$$

$$\frac{\partial \tilde{s}}{\partial t} + \tilde{u}_j \frac{\partial \tilde{s}}{\partial x_j} = - \frac{\partial \pi_{sj}}{\partial x_j} + S_s. \quad (23)$$

In the above expressions, a filtered variable μ is denoted as $\tilde{\mu}$. \tilde{u}_i is the resolved (filtered) velocity field ($i=1,2,3$); x_i is the position vector; τ_{ij} is the anisotropic part of the subgrid-scale (SGS) stress tensor; $f_c = 1.4 \times 10^{-4}$ is the Coriolis parameter; u_j^G is a large scale pressure forcing imposed in terms of a geostrophic wind; π_{sj} is the SGS scalar flux, and S_s represents volumetric sinks/sources of the scalar s . A modified resolved dynamic pressure, p^* , is defined to include the resolved and SGS turbulent kinetic energy (Bou-Zeid et al., 2005). The reference density is taken as 1 and is thus omitted from the equations. The term D_i represents the drag force exerted by the canopy elements on the flow and was computed as

$$D_i = -C_D a \tilde{u}_i |\tilde{u}_i|, \quad (24)$$

where C_D is the drag coefficient and a is the leaf-area density. The drag coefficient was modeled following Pan, Follett, et al. (2014),

$$C_D = \min \left((\langle \tilde{u}_i \rangle / A)^B, C_{D,\max} \right), \quad (25)$$

where A is a velocity scale, B a negative power-law exponent, and $C_{D,\max}$ the maximum drag coefficient. This formulation represents the change in canopy drag caused by the variation in the wind speed, which can cause the canopy elements to bend, thus modifying the canopy resistance through the drag coefficient. As shown by Pan, Follett, et al. (2014), this drag model improves the representation of higher order statistics. However, the parameters A , B , and $C_{D,\max}$ are canopy dependent and can be experimentally found if data are available. For our numerical study, we conducted various simulations for different combinations of the parameters tested by Pan, Follett, et al. (2014). We selected the parameters that resulted in the best comparison between the simulation and the velocity statistics profiles from Su et al. (1998) (more details in the section 3.1.2). The best match was observed for $A = 0.22$ m/s, $B = -1$, and $C_{D,\max} = 0.3$.

The SGS stress is modeled using the scale-dependent Lagrangian dynamic model (Bou-Zeid et al., 2005), where a constant turbulent SGS Prandtl number of 0.4 is used to infer the SGS diffusivity and compute the unresolved scalar fluxes. To ensure that the velocity field satisfies the continuity equation, a Poisson equation is solved for pressure p^* at every time step. The vertical derivatives are computed by a second-order centered finite difference scheme, implemented on a uniform staggered grid, while a pseudo-spectral method is implemented for horizontal derivatives. Finally, the explicit second-order Adams–Bashforth method is used for time stepping.

The horizontal boundary conditions are periodic. At the top, we imposed a stress term, $(\tau_{xz}, \tau_{yz}) = (u_S^2 \cos \alpha, u_S^2 \sin \alpha)$, where u_S is the kinematic stress magnitude and α is the angle between the stress vector and the x -axis. Following the steps in Zahn and Bou-Zeid (2023), we used $u_S = 0.3$ m/s and $\alpha = 174^\circ$. In addition, we imposed a stream-wise large-scale pressure forcing $(u^G, v^G) = (8, 0)$ m/s. Finally, we simulated constant flux profiles for all scalars by imposing an SGS flux (sink or source) as the top boundary condition for c and q matching the total flux magnitude imposed inside the domain (ground + canopy).

As previously discussed (Su et al., 1998; Watanabe, 2004; Zahn & Bou-Zeid, 2023), the inclusion of a top stress (and/or scalar flux) results in strong velocity and scalar gradients near the top boundary. However, Watanabe (2004) also showed that their region of interest ($\approx 70\%$ of the lower domain) was unaffected, resulting in the same turbulence statistics of a pressure-driven flow. To confirm this finding, we ran individual simulations driven by a non-zero top stress or by an imposed pressure force, confirming Watanabe (2004)’s results and also verifying that the partitioning results were consistent and independent of the choice of the top boundary condition or flow forcing. Nonetheless, we confine our analyses to the bottom part of the domain, $z \leq 5h$ ($\approx 65\%$ of domain depth).

3.1.1 Simulating plant and soil contributions of CO_2 and H_2O

One of the main goals of our simulations is to reproduce (and sample) c and q under different combinations of canopy and soil fluxes. This would require running several simulations where the contributions from the various sinks and sources vary. Not only would this be computationally expensive, but it would also likely cover only a limited area of the phase space between T/E and P/R . An easier approach, as adopted by Klosterhalfen, Moene, et al. (2019) is to obtain solutions for canopy and soil separately, and then leverage the linear nature of equation (23) that allows solution superposition to reconstruct the results based on different imposed fluxes. Following this idea, we solve this scalar balance equation separately for plant (c_p and q_t) and soil (c_r and q_e) scalars, where $c = c_p + c_r$ and $q = q_e + q_t$. Thus, only plant components have a source or sink term representing canopy transpiration and photosynthesis, while their bottom wall boundary condition is set to zero flux. Soil components, on the other hand, have an imposed surface flux at the bottom representing evaporation and respiration.

After simulating all four scalars separately, we can then recover the desired turbulent statistic for c and q . In addition, we can easily adjust the respective contributions of soil and plant components by first multiplying the original statistics of c_p , c_r , q_t , and q_e by the respective scaling factors. Note that this is only possible if q is treated as a passive scalar (otherwise the buoyant feedback from q on u_i will render the advective term in the scalar equation non-linear in q). Thus, all our simulations are neutral with respect to q . To further decrease the complexity of our simulations and interpretation of results, we also considered the flow neutral with respect to temperature, thus simulating a fully neutral canopy flow.

3.1.2 Domain configuration and data sampling

A summary of the main details of our simulations is shown in table 1. The domain contains $(N_x \times N_y \times N_z) = (384 \times 256 \times 128)$ grid points, and aspect ratios $(L_x/L_z, L_y/L_z) = (3, 2)$, where L_z is vertical domain height. This setup results in $dx = dy = dz$. In addition, the ratio of the domain height to the canopy height, h , is $L_z/h = 8$, which is in the range ($L_z/h = 3\text{--}14$) commonly adopted in the literature for canopy flows (Shaw & Schumann, 1992; Su et al., 1998; Watanabe, 2004; Yue et al., 2007; Dupont & Brunet, 2008; Mao et al., 2008; Pan, Chamecki, & Isard, 2014; Chen et al., 2020). Additional simulations with different domain height, aspect ratios, grid resolution, mean flow forcing, and soil roughness length z_0 all indicated that the partitioning results are not sensitive to the design of the domain.

The analyses shown in this study used both spatial and temporal statistics. The spatial statistics (averaged in the cross-stream direction and time) were sampled after the kinetic energy and the flux profiles reached equilibrium. For the temporal statistics, we also included 24 virtual “eddy-covariance towers” across the domain, where the velocity and all simulated scalars were sampled at all vertical grid points every 25 time steps (i.e., every 0.25 s). This is sufficient here since the smallest resolved eddy is $\sim 2dx = 2$ m and its advective time across a grid node at a mean wind speed of 1 m/s (see ve-

Table 1. Parameters of our simulations. L_z , L_y , and L_x (m) are the dimensions in z , y , and x directions; N_z , N_y , and N_x are the number of grid points in the three directions, while N_h is the number of grid points representing the canopy; dx , dy , and dz are the grid resolution; h (m) is the canopy height; u_S is the imposed friction velocity at the domain top (m/s); z_0 (m) is the roughness length of the soil surface; LAI is the leaf-area index; dt is the time step (s).

Simulation parameter	Units	Value
N_x, N_y, N_z		384, 256, 128
N_h		16
L_z	m	140
$L_x/L_z, L_y/L_z$		3, 2
$dx/dz, dy/dz$		1, 1
L_z/h		8
z_0/h		0.00285
u_S	m/s	0.3
LAI	m^2m^{-2}	2.0
dt	s	0.01

locity profiles in A1) is thus 2s; we thus sample the smallest eddies with 6 points. To ensure convergence of the time series, we sampled over a period of approximately 20 eddy turnover times (L_z/u_*).

To represent the canopy, we used the leaf-area density and the source profiles S_q (Figure 2) for water-vapor mixing ratio following Shaw and Schumann (1992) and Su et al. (1998). As in these studies, we also set the leaf-area index (LAI) to 2. The same source profile shown in Figure 2 was rescaled and used as a source for transpiration in the transport equation for q_t , and as a sink for photosynthesis in the equation for c_p .

A homogeneous forest was first simulated by imposing a drag force and scalar sources/sinks at every horizontal grid point of the first 16 vertical levels. To investigate how the sparseness of the canopy influences the partitioning methods, we designed two new domains. The first domain replicates a vineyard (Figure 3) with rows oriented parallel to the y axis. The ratio of the width of the vegetation rows (r_v) to the width of the bare soil rows (r_s) is 0.81, where $r_v/h=0.639$ and $r_s/h=0.77$. The second domain is representative of a sparse orchard, where “clusters” of vegetation of length $r_v \times r_v$ are separated horizontally from other clusters by a distance r_s . In both cases we kept the same canopy leaf-area density ($LAI=2$); thus, the effective leaf-area density is $LAI_e = LAI(A_v/A_t)$, where A_t is the total area of the xy plane and A_v is the area occupied by canopy elements. For the first and second domains, we thus have $LAI_e=0.98$ and 0.42 , respectively. In addition, the same canopy flux profiles and leaf-area density (Figure 2) were imposed. As boundary condition, we imposed a homogeneous soil flux, *i.e.*, the same respiration and evaporation magnitudes being emitted from under the canopies, as well as from the exposed soil. Simulations with heterogeneous soil fluxes were tested, but are not shown here since the key conclusions remained the same. In addition, we found no sensitivity in the results based on the location of the towers (*i.e.*, vegetated grid cell versus a bare soil grid cell). The mean wind profile and kinetic energy resultant from all three domains are shown in the Supplementary Information, Figure S1.

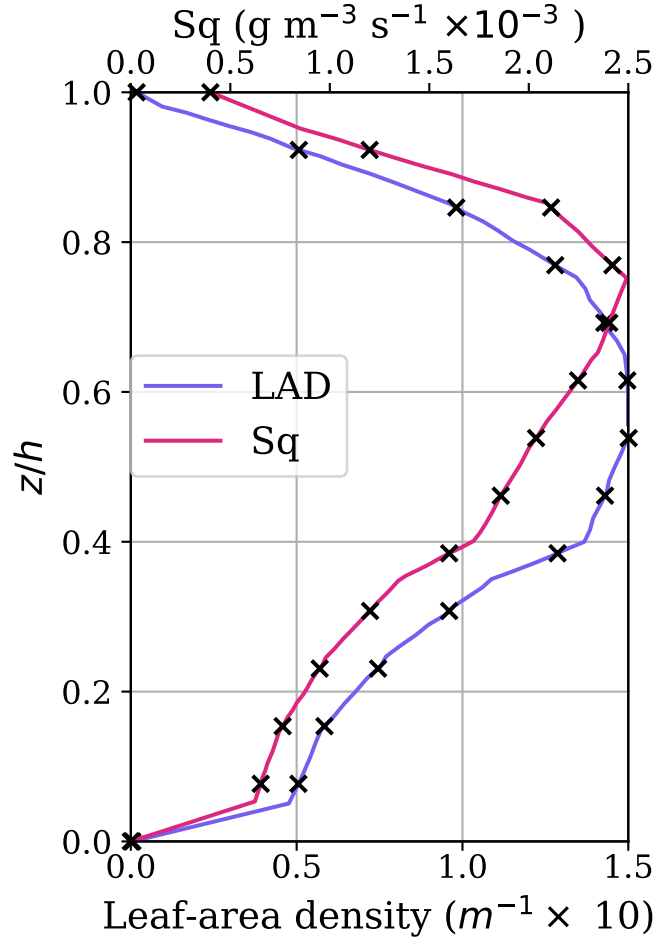


Figure 2. Leaf-area density and source profile for water vapor mixing ratio imposed in the LES (Shaw & Schumann, 1992; Su et al., 1998). The crosses indicate the values used in the numerical simulations.

To validate our LES setup, we followed Su et al. (1998) and compared our numerical results with field experimental data from Shaw et al. (1988) over a sparse forest (LAI \approx 2). This simulation was neutral with an LAD and source profiles (only water vapor) as shown in Figure 2. In addition, the lower boundary condition for water vapor was zero surface flux given the negligible evaporation at the experimental site.

A comparison between our LES results and the experimental data is included in the appendix (Figure A1). Along with the spatial statistics, we also show the temporal statistics computed as the ensemble average across the 24 towers in the domain. Good agreement is seen between spatially and temporally averaged results for all statistics. In particular, both spatial and temporal results for quadrant flux fractions (quadrant analyses) of momentum and water vapor are very similar and follow the experimental trends well. In addition, while not directly used by the partitioning algorithms, the skewness of u and w using a dynamic drag model are in better agreement with observations than when a constant drag coefficient is used (comparison not shown here). Overall, we can conclude that the time series are converged and can be used for partitioning as described next.

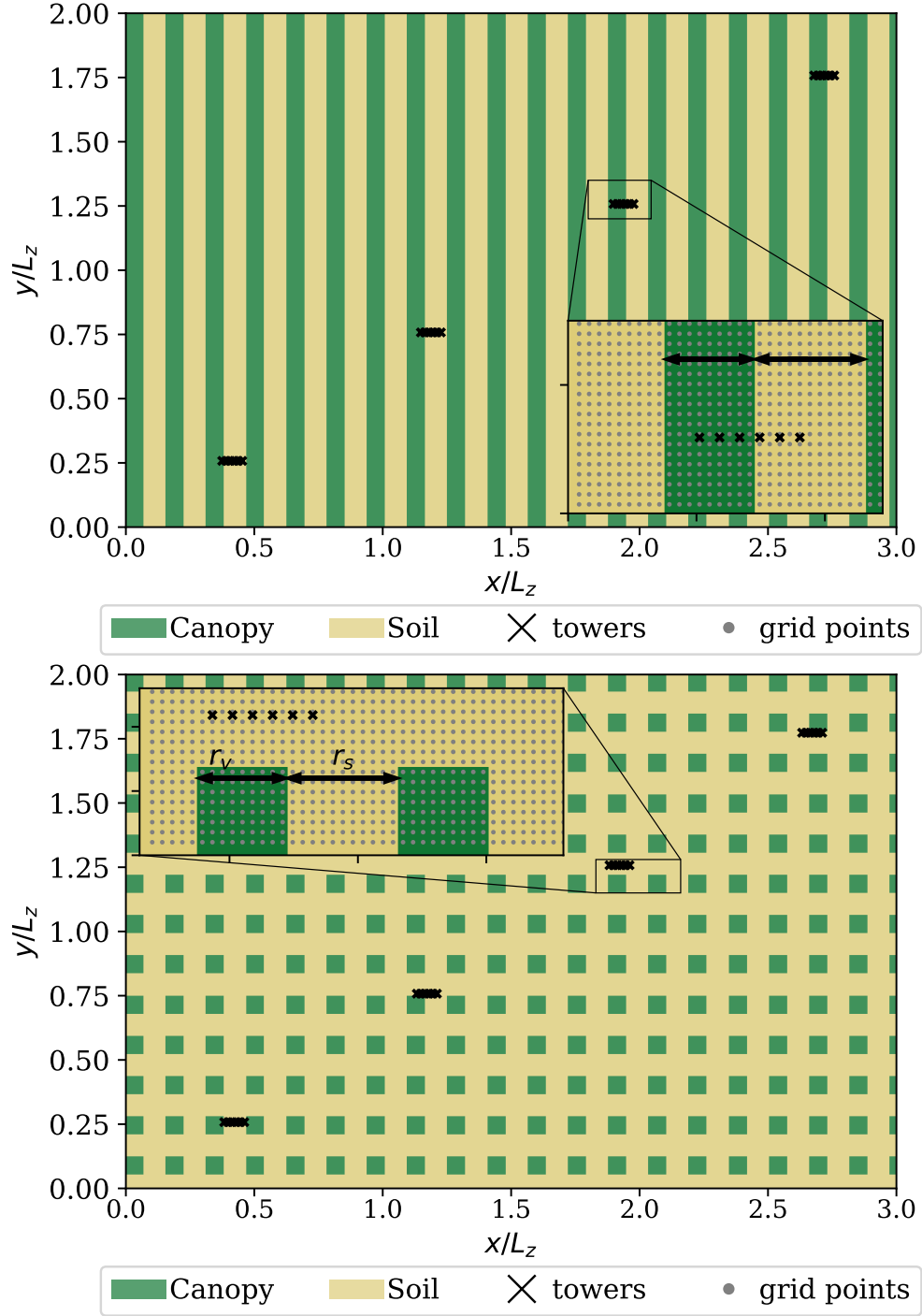


Figure 3. LES domain representing a vineyard (top) and clusters of trees (bottom).

3.2 Implementation of partitioning methods

Following the simulation and sampling of time series, we implemented all partitioning methods following the same steps as in field experiments. For FVS and CECw, we used the “real” water-use efficiency, which is imposed in the simulation. The flux components computed at every vertical grid point for all 24 towers were later averaged, resulting in one single profile for all four components and all four methods. The variability around the average values is illustrated in Figure S2 of the Supplementary Information.

As previously explained, our LES setup allows us to reconstruct the time series of c and q that would result from any combination of ET and F_c flux components. To investigate as many combinations as possible — from stronger soil fluxes to fluxes dominated by canopy components — we linearly increased T/ET by increments of 0.025 from 0 to 1, while keeping T constant. Similarly, the ratio P/RP , where we defined $RP = R + |P|$, was increased from -1 to 0, in increments of 0.025, as P was kept constant. Note that RP uses the absolute value of photosynthesis to ensure a ratio smaller than unity. Thus, the water-use efficiency remains the same for each of the 1600 flux combinations we generate.

The performance of each method was quantified by computing the biases of the canopy flux components. More specifically, we compute the bias of the flux ratios (T/ET and P/RP) as follows,

$$\text{bias}_{T/ET} = \frac{T - T_{\text{part}}}{ET}, \quad (26)$$

$$\text{bias}_{P/RP} = \frac{P - P_{\text{part}}}{RP}, \quad (27)$$

where T and P are the imposed transpiration and photosynthesis fluxes that we wish to retrieve in the partitioning, while T_{part} and P_{part} are the flux components obtained by any of the four partitioning methods (FVS, CEC, CEA, and CECw). Note that the bias computed for F_c components is not traditional in the sense that RP is not a physical quantity, but it was here defined in analogy with ET as a way to avoid division by zero whenever $P \approx -R$. This bias offers more insightful information, compared to one normalized with F_c , regarding the best estimates of P .

4 Results and Discussion

We start this section by discussing the impact of canopy sparseness on transport efficiency; in particular, how the presence of gaps, or “canyons”, influence turbulence mixing, and what are the implications for flux partitioning. We follow the discussion by investigating the performance of each partitioning method for different measurement heights, flux component strength combinations, and canopy sparseness. We conclude our analyses by illustrating how turbulence data can be helpful in understanding biophysiological variables, such as the water-use efficiency.

4.1 Effect of canopy sparseness on mixing efficiency

A common feature across all four partitioning methods is their requirement of a degree of uncorrelatedness between soil and plant flux components: the parcels emanating from the soil and plants cannot be well mixed (correlated) if the separate signals are to be captured. The CEC, CEA, and CECw methods further require the presence of eddies that were in contact with the soil, and were subsequently transported to the sensor level without being fully mixed. Therefore, one expects that plant canopies with exposed gaps, such as vineyards, would offer a suitable environment for these methods. To explore the differences in turbulent statistics in different plant canopy configurations, we show in Figure 4 the correlation coefficient between c_r and c_p , namely ρ_{c_p, c_r} , as well as

the skewness (Sk_{c_p} and Sk_{c_r}) of both quantities obtained from simulations over a homogeneous canopy, a vineyard, and a cluster domain. Note that ρ_{c_p, c_r} is here used as a measure of the degree of mixing between soil and canopy air parcels; for instance, in the event when $\rho_{c_p, c_r} = -1$, the parcels are fully mixed and no relevant partitioning information can be extracted.

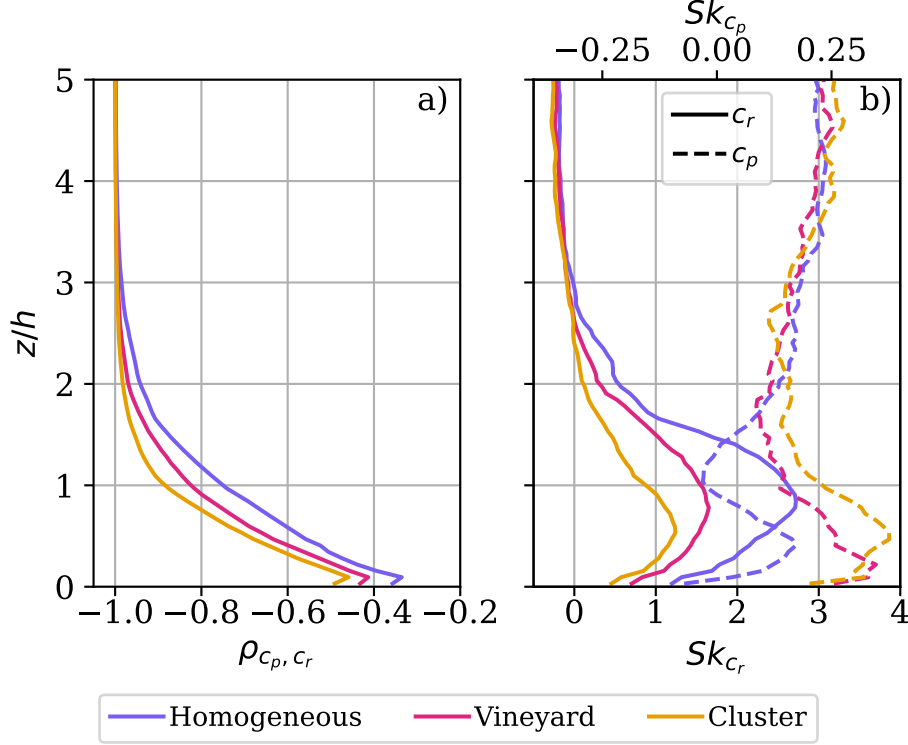


Figure 4. Correlation between soil and plant components, and their individual skewness, over homogeneous and heterogeneous canopies. Note that part (b) has a top and bottom x -axes.

As shown in Figure 4a, the correlation between soil and plant components approaches -1 at lower levels above the vineyard and the cluster domains. The implication is that soil respiration is mixed faster and at a lower height above the soil when wide gaps between plants are present. This, it turns out, is due to stronger shear turbulence generation by the gaps, compared to the homogeneous setup. Therefore, ejections enriched in CO_2 , representing the soil surface, are more likely to be sampled before being fully mixed into the flow over the homogeneous canopy. Figure 4b further corroborates this argument by indicating greater skewness for c_r in the homogeneous domain at $z/h < 2$. In this case, greater skewness indicates that more parcels were sampled with high c_r values as a result of ejections carrying parcels enriched in CO_2 . The same is true for Sk_{c_p} , shown to be negative at the canopy top over the homogeneous case. Figure 4b also indicates that scalars emitted by the canopy distributed profile have smaller skewness magnitudes than the scalar emitted at ground level due to stronger mixing inside the canopy. According to Edburg et al. (2012), strong and intermittent organized turbulence structures penetrate the entire canopy, albeit infrequently, and cause bursts of scalars emitted from the soil.

Overall, these results contradict our initial expectation that exposed patches of soil improve the representativeness of soil respiration in conditional sampling analyses. In fact, they indicate that the opposite is true, *i.e.*, that the presence of wide gaps (or canyons)

increases turbulence mixing of soil fluxes, potentially worsening the performance of CEC and CEA. Nonetheless, while vegetated canopies with the presence of open canyons and gaps are non-ideal, it is still necessary that the vegetated canopy of interest be porous enough such that updrafts originating below the canopy can escape vertically. As discussed by Zahn et al. (2022), canopies that are too dense might lead to uncoupled flows and lateral advection of soil fluxes (C. K. Thomas et al., 2013) that are not only problematic to partitioning, but to flux quantification in general.

4.2 Partitioning versus flux component strength at various elevations

In this section we explore the performance of all four partitioning methods evaluated with regards to measurement height and the relative magnitude of plant and soil fluxes of CO_2 and H_2O . This analysis will then enable a more comprehensive evaluation of all methods, which previously had only been numerically explored for a few combinations of fluxes (Klosterhalfen, Moene, et al., 2019).

As expected based on the comparison of mixing efficiency across domains — indicating faster mixing of soil and canopy scalars when large gaps are present — the partitioning performance for both heterogeneous domains is slightly worse than those over the homogeneous case. Thus, we will focus on the results for the homogeneous canopy simulation, noting that the figures for both heterogeneous domains are included in the supplementary information in Figures S3–S10.

The biases in the partitioning (reported for T and P , from which the skill for E and R can be inferred since the sum of the fluxes is known in all models) computed by the FVS method are shown in Figure 5. These results clearly indicate that, as long as the water-use efficiency is known exactly and the method converges to a solution, the FVS method has an excellent performance across all flux magnitude combinations. The biases for both T and P slightly decrease from $z = h$ to $z = 3h$ as a consequence of the smaller errors in the approximations in equation 1 as the scalars correlations increase at higher levels, but are still not perfect (*i.e.*, $\rho_{c_p, c_r} \neq -1$ and $\rho_{q_t, q_e} \neq +1$), as will be discussed in section 4.3. Nonetheless, over heterogeneous domains (Figures S3 and S7 of the SI) we observe regions with greater biases (≈ 0.2) as a result of strong turbulent mixing, as shown in the previous section, which also causes $|\rho_{c,q}|$ to be close to unity. Equations 2a and 2b, as well as expression 5, are sensitive to $\rho_{c,q}$ under these conditions, sometimes resulting in larger errors or lack of convergence to a realistic solution. As a reminder, for each level and each flux combination, we average the four flux components across all 24 towers; thus, in some cases (at higher levels or greater correlations), not all towers resulted in valid solutions and were not included in the average. A more detailed discussion on the sensitivity of the FVS method is presented in section 4.3 and 4.4.

The bias with regard to the correct ratio T/ET (top panel) and R/RP (bottom panel) obtained by the CEC method is shown in Figure 6. An important feature to note is that the bias is generally much smaller for the carbon components, a finding that applies to all other methods we have tested (they all partition F_c remarkably well, except when $R \approx -P$). The reason behind this smaller bias is that the sign of the CO_2 flux determines which component dominates, which is not the case for ET since both E and T are positive. For instance, $F_c < 0$ clearly indicates that P dominates. CEC, CECw, and CEA, by construction, assume that greater or smaller P also entails greater or smaller T (*i.e.*, constant water use efficiency with typical, not too small or large, values). Thus, larger errors are expected for ET partitioning when this expectation is not met (*i.e.*, away from the 1:1 diagonal on the figures).

This can be further illustrated by focusing on $z/h = 1$, where we can identify a region with $|(T - T_{CEC})|/ET \leq 0.2$; in particular, we see that the best agreement is expected when the ratios $-P/R$ and T/E grow in tandem. On the other hand, greater errors are expected when one component overwhelmingly dominates the other. Thus, one

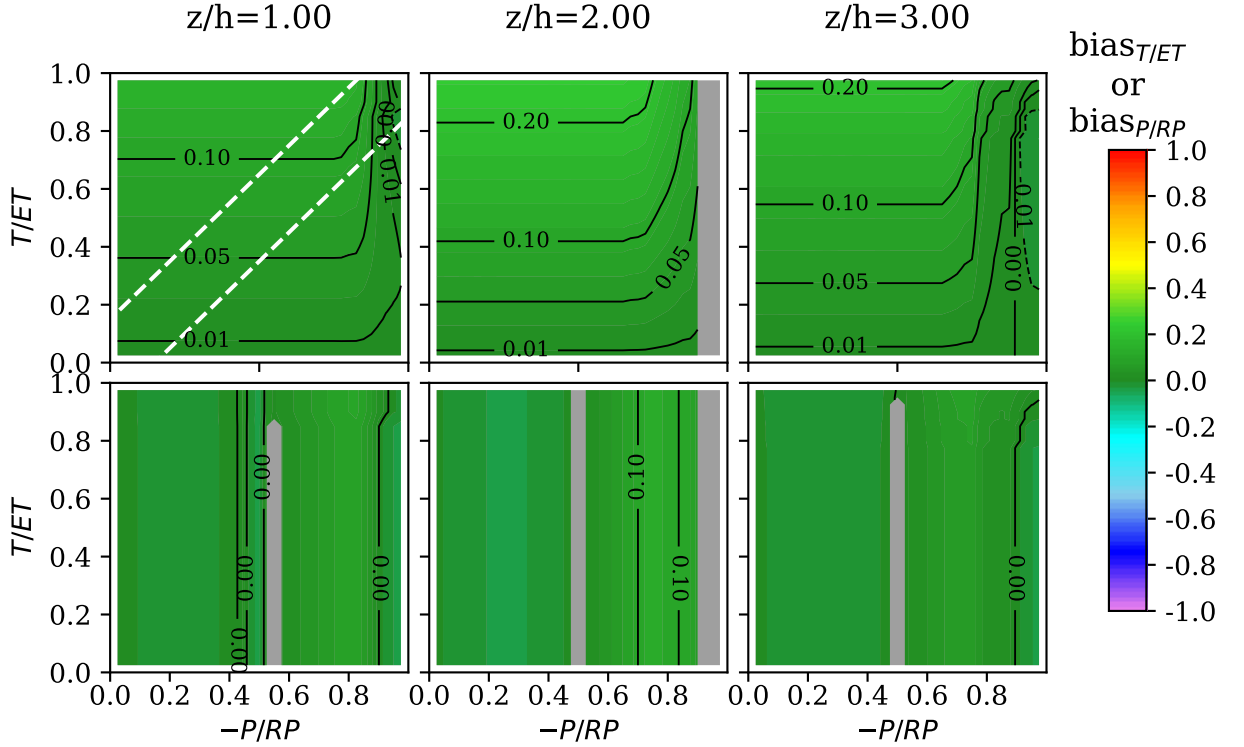


Figure 5. The top three plots show the bias in the partitioning of ET following the FVS method at $z/h = 1, 2, 3$, where the colors represent the bias in transpiration, $(T - T_{FVS})/ET$. Bottom plots show the bias for CO₂ components, defined as $(P - P_{FVS})/RP$, where $RP = R + |P|$. Regions in gray represent combinations where no physical solutions were found because $R_{FVS} \approx -P_{FVS}$. Flux combinations inside the area delimited by the white dashed lines represent the condition $-P/RP - 0.15 < T/ET < -P/RP + 0.15$, from which we will later select points for further analysis. Colorbar is limited to ± 1 for easy comparison with subsequent figures.

requirement for good performance of CEC is that the ratios P/T and R/E should not be too dissimilar. However, note that regions where $|(T - T_{CEC})|/ET \geq 0.4$ correspond to flux combinations that are unusual or physically improbable. For instance, the top left corner would indicate fluxes dominated by transpiration and respiration, but with little evaporation and photosynthesis. Such occurrence is unlikely given the expected proportionality between transpiration and carbon assimilation as defined by the water-use efficiency. Soil components, on the other hand, share physical drivers such as soil moisture and temperature, as well as turbulence intensity near the surface, but they are more loosely coupled compared to their canopy counterparts. After rain, for instance, it is possible that respiration could be suppressed by soil saturation (Xu et al., 2004), while evaporation would be large.

As we move to higher levels, the region where $|(T - T_{CEC})|/ET \leq 0.2$ becomes narrower, and good performance for CEC in partitioning water vapor flux is confined to cases when R is on the order of $-P$. Similarly, biases for Fc components increase at higher levels, but remain smaller than for water components. These results corroborate previous experimental findings (Zahn et al., 2022) suggesting that the best performance of the CEC method is achieved for measurements collected as close to the canopy as pos-

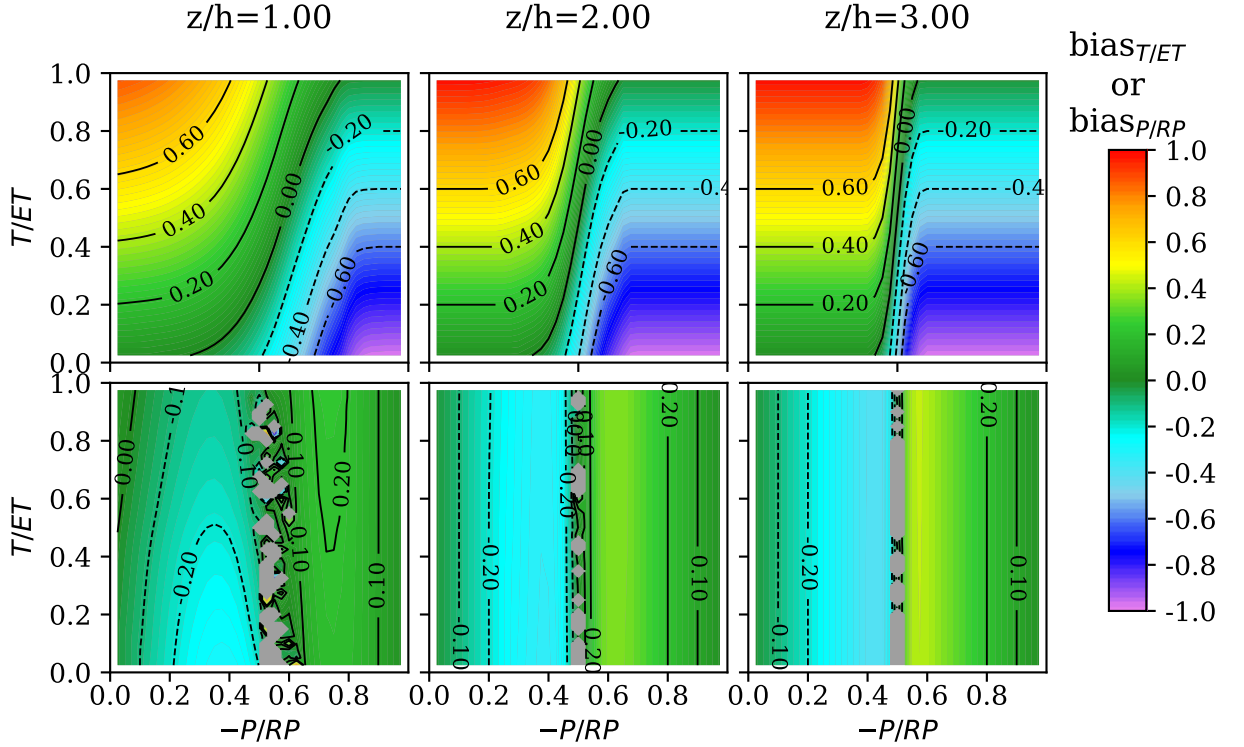


Figure 6. Same as 5, but for the CEC method.

sible, ensuring that some uncorrelatedness between the various sinks and sources is sampled.

Results for the CEA method (Figure 7) are slightly superior, but broadly similar, to CEC. The biases for ET and F_c partitioning are lower, and CEA outperforms CEC significantly at higher levels. Similarly, larger errors in ET partitioning are expected for flux combinations that are less likely to occur, for the same reason as CEC. On the other hand, F_c partitioning remains very accurate as long as the net flux is not ≈ 0 .

Lastly, we show the results obtained with the CECw method. Interestingly, despite similar assumptions to CEC, it performs better than the former in partitioning ET , displaying a wider range where biases are smaller than 20% and consistent performance at least up to $z/h = 3$. Further, its performance in partitioning F_c is also quite different from CEC or CEA, with much better performance when $R \approx -P$, and worse performance away from the 1:1 diagonal. Note that these results are also dependent on prior knowledge of the water-use efficiency, and thus the performance of the CECw method share this shortcoming with the FVS method. In addition, although not performing as well as FVS when W is known, the CECw method is easier to implement and its poor performance, e.g. where $(T - T_{CECw})/ET \geq \pm 0.4$, is restricted to regions with unlikely flux combinations as with CEC and CEA. Such result highlights the importance of the water-use efficiency for more accurate ET partitioning estimates. In this regard, even a simpler approach, such as CECw, can yield reliable results when W is known. In addition, as long as CO_2 fluxes are not mostly dominated by respiration — where the method did not find valid solutions, as shown in Figure 8 — CECw does not suffer from the same convergence issues as reported for the FVS method in previous studies. Thus, CECw seems to be a good complement to the FVS method, ensuring a complete record of flux components that are consistent with the WUE that both methods require. Yet,

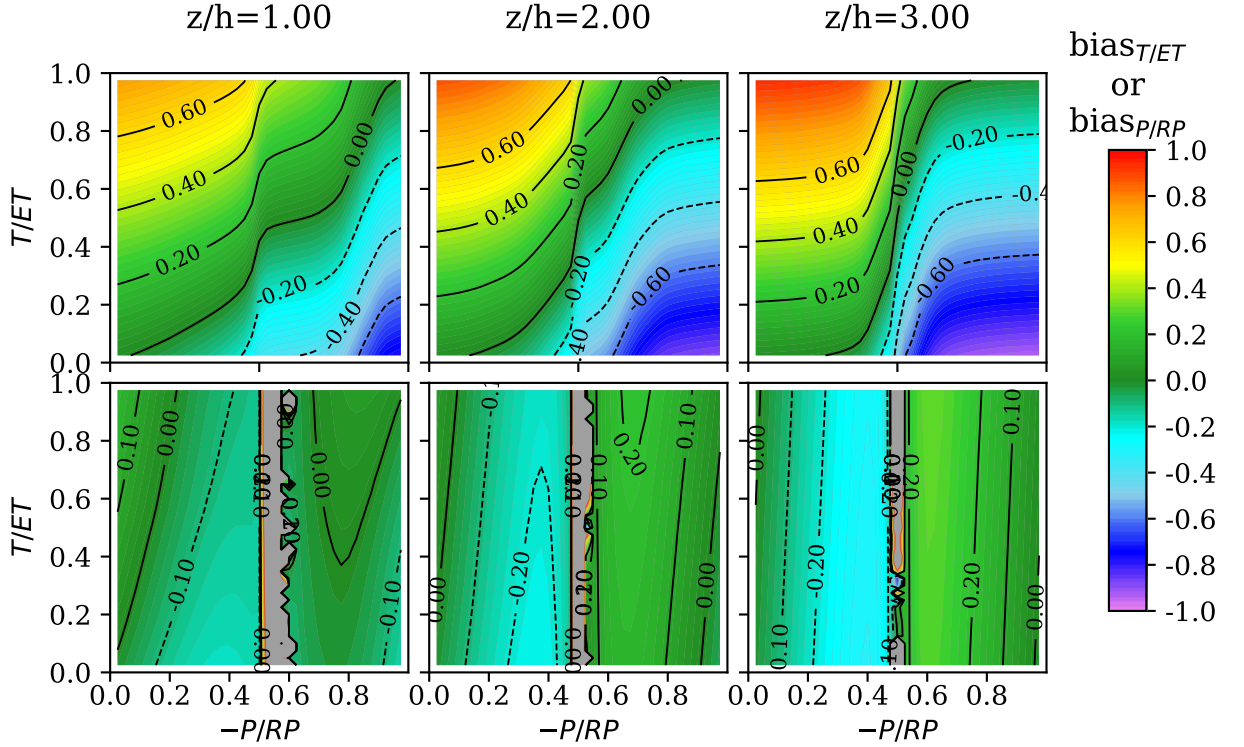


Figure 7. Same as 5, but for the CEA method.

the resulting complete record will also be subject to the uncertainty that results from uncertainty in WUE.

4.3 Revisiting physical assumptions

One of the main advantages of investigating the partitioning methods through numerical simulations is the possibility of assessing their physical and mathematical assumptions. By simulating all four scalars separately, we are now able to investigate if the approximations adopted by Scanlon and Sahu (2008) and Scanlon and Kustas (2010) in their mathematical derivation, as well as the assumption of eddies enriched in CO_2 coming from the soil, invoked for both CEC and CEA, are appropriate.

The expressions given by equation (1) represent the main source of uncertainty in the FVS method (not considering the ability to estimate W). These approximations assume that the correlation coefficient between plant and soil CO_2 (ρ_{c_p, c_r}) can be estimated as the ratio of their respective transfer efficiencies ($\rho_{w, c_p} / \rho_{w, c_r}$), the same applying to H_2O components. Such approximation was first proposed by G. Katul et al. (1995) in their study of similarity between temperature and water vapor. Bink and Meesters (1997) later demonstrated that $\rho_{T, q} \approx \rho_{w, T} / \rho_{w, q}$ can yield satisfactory results as long as $\rho_{w, T} < \rho_{w, q}$, that is, when water vapor is more efficiently transported by turbulence than temperature; if the opposite is true ($\rho_{w, T} > \rho_{w, q}$), then the appropriate approximation is $\rho_{T, q} \approx (\rho_{w, T} / \rho_{w, q})^{-1}$.

Following the arguments of Bink and Meesters (1997), Scanlon and Sahu (2008) assumed that the transfer efficiency of plant components, c_p and q_t , are greater than the transfer efficiency of soil components, c_r and q_e , due to data sampling being done above

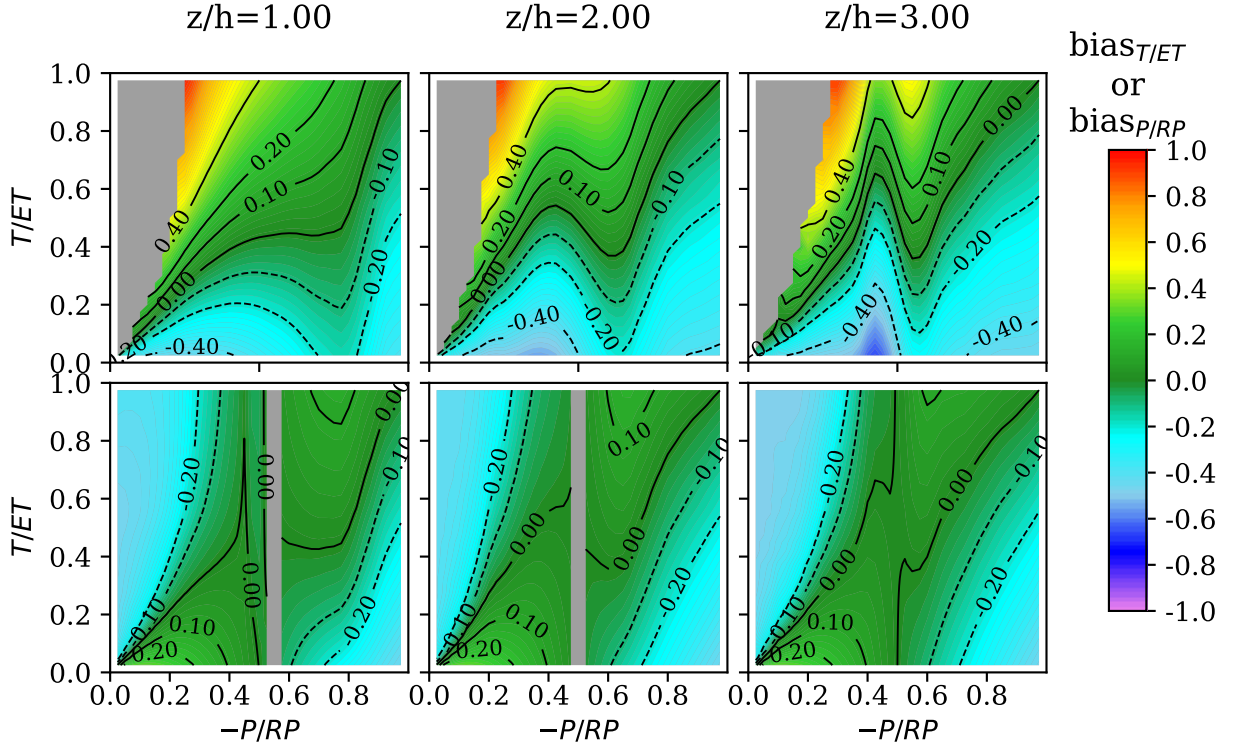


Figure 8. Same as 5, but for the CECw method.

the canopy (i.e., close to the sink of c_p and q_t). Thus, for c we need to satisfy $\rho_{w,c_p} > \rho_{w,c_r}$, which clearly implies $|\rho_{c_p,c_r}| \leq 1$.

Figure 9 shows how this approximation (a value of 1 in the plot implying zero error) holds over a homogeneous canopy, as well as for the two sparse canopies described in 3.1.2. Results for CO_2 and H_2O are the same, thus only the former are shown. In addition, note that these results do not depend on the magnitude of soil and canopy fluxes, meaning that the same results hold regardless of the magnitude of respiration (evaporation) and photosynthesis (transpiration). Overall, it is clear that the approximation is worse below the canopy top (although less relevant since partitioning methods are not applied in this region), where the transfer efficiency of respiration is greater given the proximity to the soil. Above the canopy, on the other hand, the approximation is more appropriate, almost reaching equality. In addition, the faster convergence towards unity in sparser canopies is a consequence of the more efficient turbulent mixing in the presence of gaps, as previously discussed.

For $z/h \geq 3$, the magnitudes of the correlation ρ_{c_p,c_r} — as well as ρ_{q_t,q_e} and $\rho_{c,q}$ (not shown in the figure) — reach values close to unity for all three simulations, causing the approximation in Equation (1) to approach equality. However, the derivation of the FVS method requires $|\rho_{c,q}| < 1$ (see equation 5), i.e., it is undefined in case of perfect correlation. As expected, we verified that this constraint is not satisfied — and thus fewer valid solutions are available — more often at $z/h = 3.1$ than at $z/h = 1.5$ (Figure S13 in the Supplementary Information). In addition, this behavior was observed more often when photosynthesis dominated the total CO_2 flux, and for heterogeneous domains.

Therefore, on one hand FVS requires a degree of decorrelation between scalars; on the other hand, its mathematical approximations in equation (1) are more accurate in

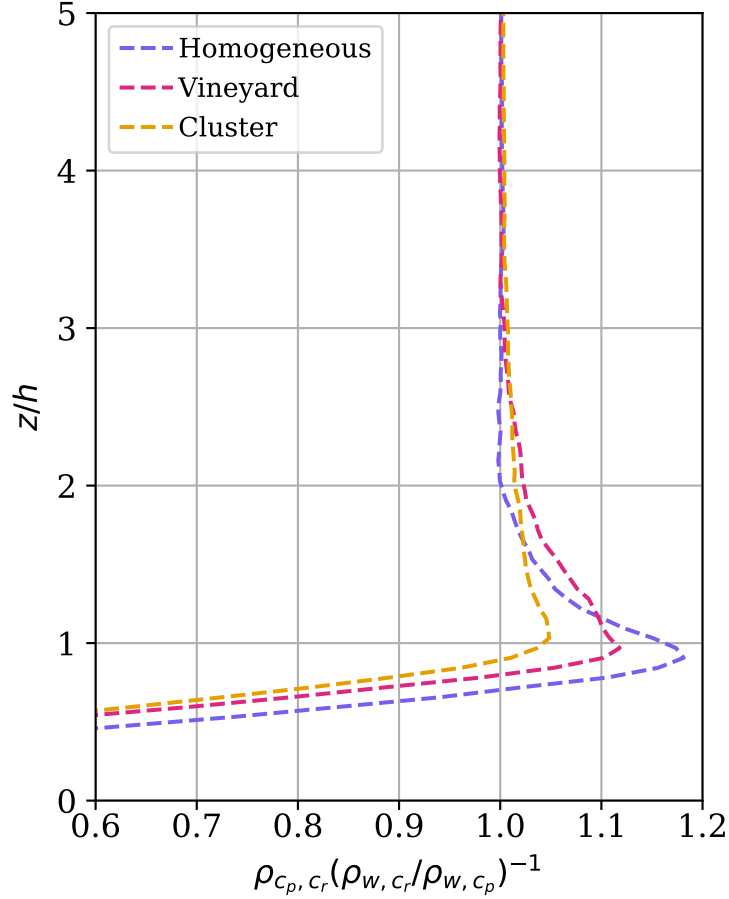


Figure 9. Profile of the ratio defined in equation (1). When this ratio reaches unity, it indicates that the approximation is valid. Profiles were obtained by averaging the correlation coefficients at each level across all 24 towers.

regions where the different scalars are better mixed and their correlations are almost perfect. These contradictory requirements, also observed by Klosterhalfen, Moene, et al. (2019), add complexity to the interpretation of field data partitioning using FVS, and potentially decrease the number of valid partitioning estimates.

A different approach to guarantee equality of expression (1) would be its multiplication by a correction factor, as done by Klosterhalfen, Moene, et al. (2019). Nonetheless, as shown by the authors, the correction values obtained from their simulations vary, and the extrapolation to real field data is impractical. Thus, we do not pursue this correction here. With the limited information we usually have from experimental data, we can only hypothesize that a measurement height where there is strong, but not complete, mixing is preferable for the FVS method, and should result in the smallest uncertainties with regards to (1).

The main assumption behind the CEC, CECw and CEA methods is that, considering that the measurements are done close enough to the sinks and sources, we are able to distinguish turbulent structures coming from the soil or from the canopy. More specifically, we are able to sample eddies enriched in CO_2 that were in contact with the surface and carry the respiration signature. These methods further expand this idea by also

considering eddies that were in contact with the canopy, and thus are depleted in CO_2 . To investigate if this assumption is appropriate, we show in Figure 10 instantaneous snapshots of c'_r , c'_p , and the total CO_2 , c' , simulated for a homogeneous domain. As a reminder, c_r and c_p were simulated separately and later used to reconstruct c . For this simulation, we set $P = -R$.

The snapshot of c_r in Figure 10d clearly shows the presence of turbulent structures enriched in CO_2 right above the surface (see for instance, $x/L_z \approx 1.5, 2.4$). These same structures persist — although with smaller concentration given the assimilation of CO_2 — in the reconstructed field of total c in Figure 10f. Similarly, we can observe regions depleted in CO_2 as a result of assimilation (e.g., $z/L_z \approx 3.0$ in Figure 10e) and that are still present in the field of total CO_2 . However, note that these structures are only distinguishable below $z/h = 3$ (white dashed line); above that level, turbulent mixing becomes stronger and we are no longer able to separate plant and soil signals. These results thus lend credibility to the assumption that we can distinguish the origin of eddies solely based on high-frequency measurements. They also support previous conclusions (Zahn et al., 2022) that CEC, and this also applies to CEA and CECw, is more likely to perform better when sampling is done as close as possible to the canopy top.

In Figures 10a–c we show an example of the quadrant analyses of a time series measured at $z/h = 1.2$. Points on the first quadrant — related to respiration ($w' > 0$, $c' > 0$, $q' > 0$) — have larger concentrations than on the second ($w' > 0$, $c' < 0$, $q' > 0$), which is related to photosynthesis. This asymmetry — evident in the skewness profile shown in Figure 4 — is caused by stronger bursts of parcels enriched in CO_2 that were “trapped” under the canopy and took longer to be ejected. Carbon assimilation, on the other hand, is the strongest at the top of the canopy (Figure 2), and thus air parcels depleted in CO_2 located around $z/h \approx 1$ are mixed faster, as indicated by the transfer efficiency of c_p . Despite the asymmetry, the quadrant plot of c shows that conditional sampling is able to distinguish between the contribution of soil and canopy eddies, and can thus be used to infer the conditional flux ratios (equation 8).

The main difference observed in the patterns over homogeneous and heterogeneous domains (vineyard and cluster, Figures S11 and S12 of the SI) is the blending height at which full mixing of flux components happens. As expected from the greater turbulent mixing efficiency in sparser canopies, ejections carrying the soil signature are shorter lived, being almost fully mixed with the flow above $z > 2h$; for the cluster-like domain these structures are only distinguishable below $z < h$. These results suggest that in very open canopies, the measurement height should be even closer to the canopy, ideally at the canopy top, to ensure the best performance possible for CEC and CEA. It is important to note that better total flux convergence, away from the influence of individual plant components, is expected away from the canopy at a height of at least $1.4h$ (Pattey et al., 2006). To avoid loss of information caused by EC measurements close to the canopy top (both for homogeneous and heterogeneous configurations), one approach would be the simultaneous placement of an EC system at $z = h$, which will be used to estimate the flux ratios (E/T and R/P), and one system further away from the effects of the canopy layer ($z > 1.4h$). By considering that the flux ratios measured at the canopy top are conserved, we can use this information to obtain converged flux components further away from the canopy.

4.4 Sensitivity of FVS and CECw to water-use efficiency

As shown in previous sections, the FVS and CECw methods are reliable partitioning approaches when the water-use efficiency is known. However, such information is usually not available from measurements, and different parameterizations of W can be implemented (Skaggs et al., 2018; Zahn et al., 2022). Wagle et al. (2021) compared different approaches to parameterize W , more specifically how to model the interstomatal CO_2

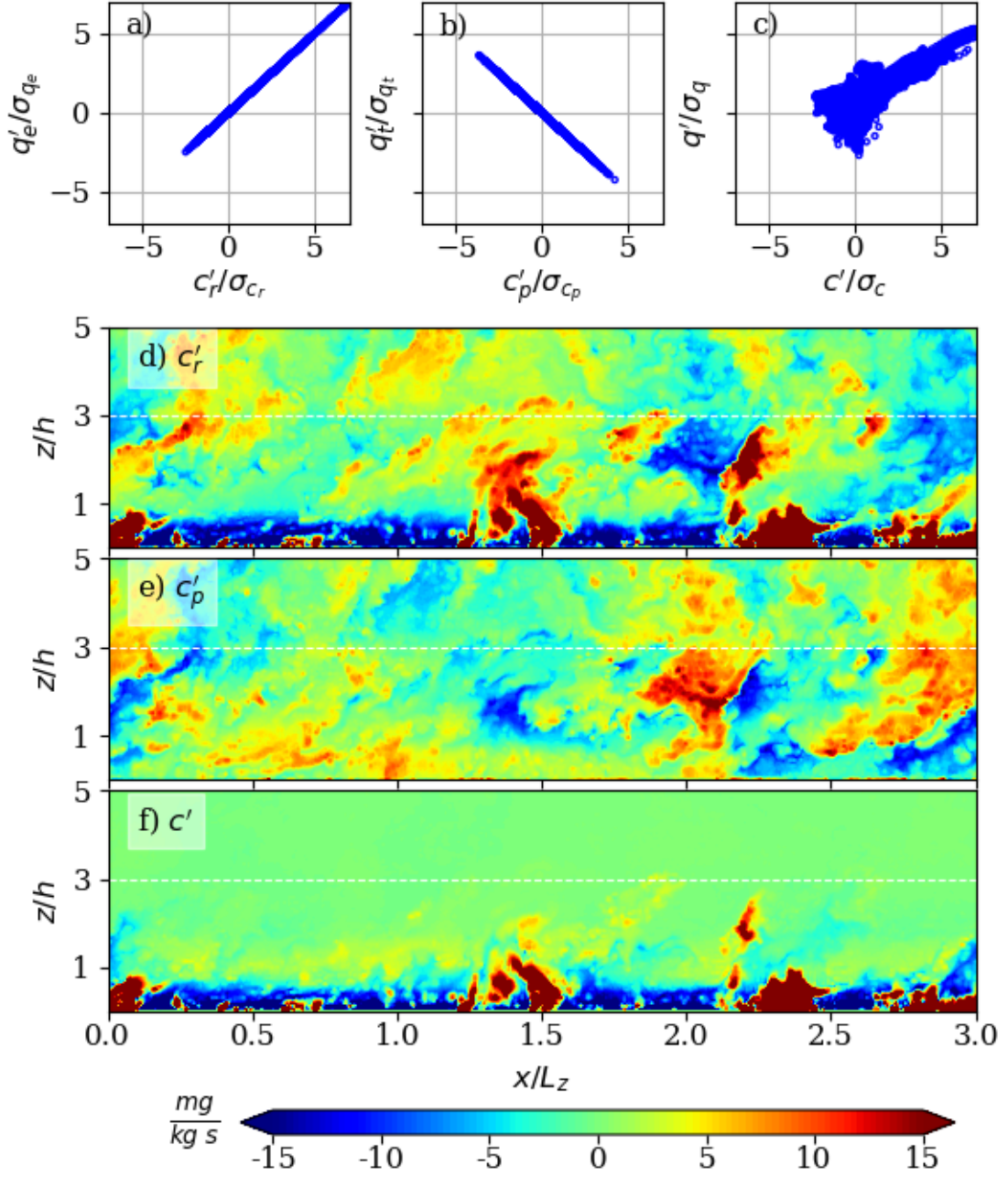


Figure 10. Panels a-c show the quadrant plot between the different components of c and q from a time series measured at $z/h \approx 1.2$. Only ejections ($w' > 0$) are included. Note that the conditional sampling implemented by the CEC is based on plot c). The bottom three panels show instantaneous fields of d) c'_r , e) c'_p , and f) $c' = c'_r + c'_p$. The white dashed line represents the height $z = 3h$. In this neutral simulation over a homogeneous canopy, $R = -P = 1 \text{ mg m}^{-2} \text{s}^{-1}$.

764 concentration, finding that the variability across different W models depends on the type
 765 of crop.

To investigate the sensitivity of both methods to uncertainties in the water-use efficiency, we repeated the partitioning with FVS and CECw after increasing W by up to 100% or reducing it by up to 90%. That is, the water-use efficiency fed to both methods, W_{input} , was increased by up to 2 times or reduced to 0.1 times its original value, W_{real} , used in LES to generate the time series. This range was selected based on the variability detected for W using different parameterizations (Zahn et al., 2022; Wagle et al., 2020) and thus represent uncertainties expected in field experiments. Large variability is also expected for different biomes and plant species as shown in the summary by Fatichi et al. (2022), where W was found to vary by a factor of five across different vegetation types.

The sensitivity of FVS and CECw to water-use efficiency is shown in Figure 11, where two examples with different flux components are presented. In both cases, T_{FVS} increases/decreases by $\approx \pm 50\%$ as W changes by $\pm 90\%$ of its original value at $z = 1.7$. P_{FVS} , on the other hand, departs faster from its correct value when the water-use efficiency is overestimated. For instance, $P_{\text{FVS}}/P \approx 0.5$ when W increases by 50%, while $P_{\text{FVS}}/P \approx 1.25$ when W decreases by 90%. In contrast to FVS, T_{CECw} is less sensitive to changes in W , while P_{CECw} rapidly departs from the true value as the water-use efficiency decreases or increases. In addition, results for CECw are also dependent on the magnitude of the different flux components (compare plots 11b and 11d), and thus generalization to other conditions is more challenging.

To illustrate how the sensitivity of these methods to W vary with different flux magnitude combinations, we plot a phase diagram for biases in T and P obtained by FVS (Figure C1) and CECw (Figure C2) when W varies from 100% to -50% of its original value. Not only T_{part} and P_{part} vary in opposite directions, which is expected given their connection through W , but over/underestimation is governed by the combination of T/ET and P/RP ratios, as well as by whether W is over/underestimated. For FVS, larger errors are expected when W is over/underestimated under conditions when canopy fluxes dominate (see upper right corners in Figure C1).

Besides having W as an input, the implementation of the FVS method requires the correlation coefficient between q and c as well as their variances. As a consequence, errors in the time series associated with field measurements, sensor limitations, as well as as post-processing data techniques, are further sources of uncertainty to partitioning estimates. For instance, Detto and Katul (2007) show that the necessary density effect corrections (DEC) of the c and q time series measured by open-gas analyzers greatly impact all their higher order statistics, in particular for c . Gao et al. (2020), on the other hand, criticizes DEC, suggesting that it affects the high frequencies of the c spectra, impacting similarity between scalars and their statistics. Thus, because the FVS method directly relies on σ_c and $\rho_{c,q}$, its performance is likely influenced by uncertainties in these corrections, which potentially impact the number of valid solutions found as has been reported in other studies (Sulman et al., 2016; Klosterhalfen, Graf, et al., 2019; Zahn et al., 2022). In these cases, solutions were not found when expression (5) was not satisfied. However, further investigation of this hypothesis and quantification of such errors are left for other studies since it cannot be easily replicated in large-eddy simulations.

4.5 Connecting biophysiological variables to turbulence statistics

In this section, we explore the connection between the water-use efficiency, as imposed in our simulations, and the correlation coefficient $\rho_{c,q}$ retrieved from the final simulated turbulence data. Figure 12a shows the variation of W/W_f , where we defined a “total” flux water-use efficiency $W_f = F_c/ET$, with $\rho_{c,q}$ at four heights above the canopy. In addition, for all heights, we only show flux component combinations presented on the phase diagrams when $-P/RP - 0.15 < T/ET < -P/RP + 0.15$ (see dashed lines in the first plot of Figure 5). This constraint not only selects periods when all methods per-

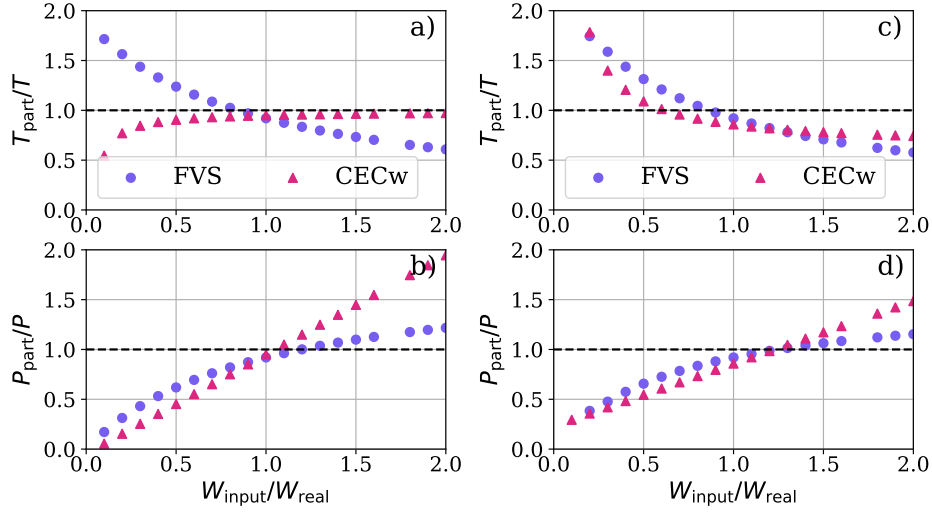


Figure 11. Sensitivity of the FVS and CECw methods to variability in the water-use efficiency at $z/h=1.7$, where W_{input} is the water-use efficiency used for partitioning, while W_{real} is the water-use efficiency imposed in the simulation. Panels a) and c) show how transpiration varies, while panels b) and d) show results for photosynthesis. Simulation on the left side correspond to $T = E=50 \text{ Wm}^{-2}$, $P = 1 \text{ mg m}^{-2}\text{s}^{-1}$, and $R = 1.1 \text{ mg m}^{-2}\text{s}^{-1}$. Fluxes imposed in the simulation shown on the right were $T=65 \text{ Wm}^{-2}$, $E=50 \text{ Wm}^{-2}$, $P = 1.7 \text{ mg m}^{-2}\text{s}^{-1}$, and $R = 1.1 \text{ mg m}^{-2}\text{s}^{-1}$.

formed well, but also removes the most “unphysical” or rare flux component combinations.

First we note that $W/W_f = (1 + E/T)(1 - R/P)^{-1}$; therefore, $W/W_f > 0$ implies $R < P$ while $W/W_f < 0$ implies $R > P$. A stronger connection between $W/W_f > 0$ and $\rho_{c,q}$ is noticed at the top of the canopy, with W/W_f increasing as the correlation increases from -1 to ≈ 0.5 . The same trend is still visible at $z/h = 2$, although it is less “continuous”, with the presence of “gaps”, as we go above this level. Overall, for $W/W_f > 0$, the increase of respiration or evaporation both invariably lead to an increase in W/W_f given that $W_f = Fc/ET$ decreases when R increases (for a constant P) or when E increases (constant T). However, when $W/W_f < 0$, a further increase in R leads to a decrease in the ratio W/W_f , while an increase in E causes its increase (arrows in Figure 12a). The transition in the sign of W/W_f occurs at different values of $\rho_{c,q}$ depending on the height, but clearly the ratio of water-use efficiencies is better defined when canopy components dominate the total fluxes and $W/W_f > 0$.

The relation between T/ET and $\rho_{c,q}$ is shown in Figure 12b. CEC predicts a good agreement, on average, with the true T/ET ratios, while CEA underestimates the true ratios (note that CEA outperforms CEC in other regions of the phase diagram that were not included following the condition $-P/RP - 0.15 < T/ET < -P/RP + 0.15$). The CECw method clearly diverges from the expected trends for $\rho_{c,q} > 0.50$, performing similarly to the other methods when plant components become more important. Regarding the FVS method, it underestimates T/ET when $\rho_{c,q}$ is very negative, *i.e.*, when the CO_2 fluxes are strongly dominated by photosynthesis, but closely follows the expected LES (simulated) values as the correlation coefficient becomes positive. Overall, the relation between the ratios T/ET and $\rho_{c,q}$ follows the behavior shown in our previous study

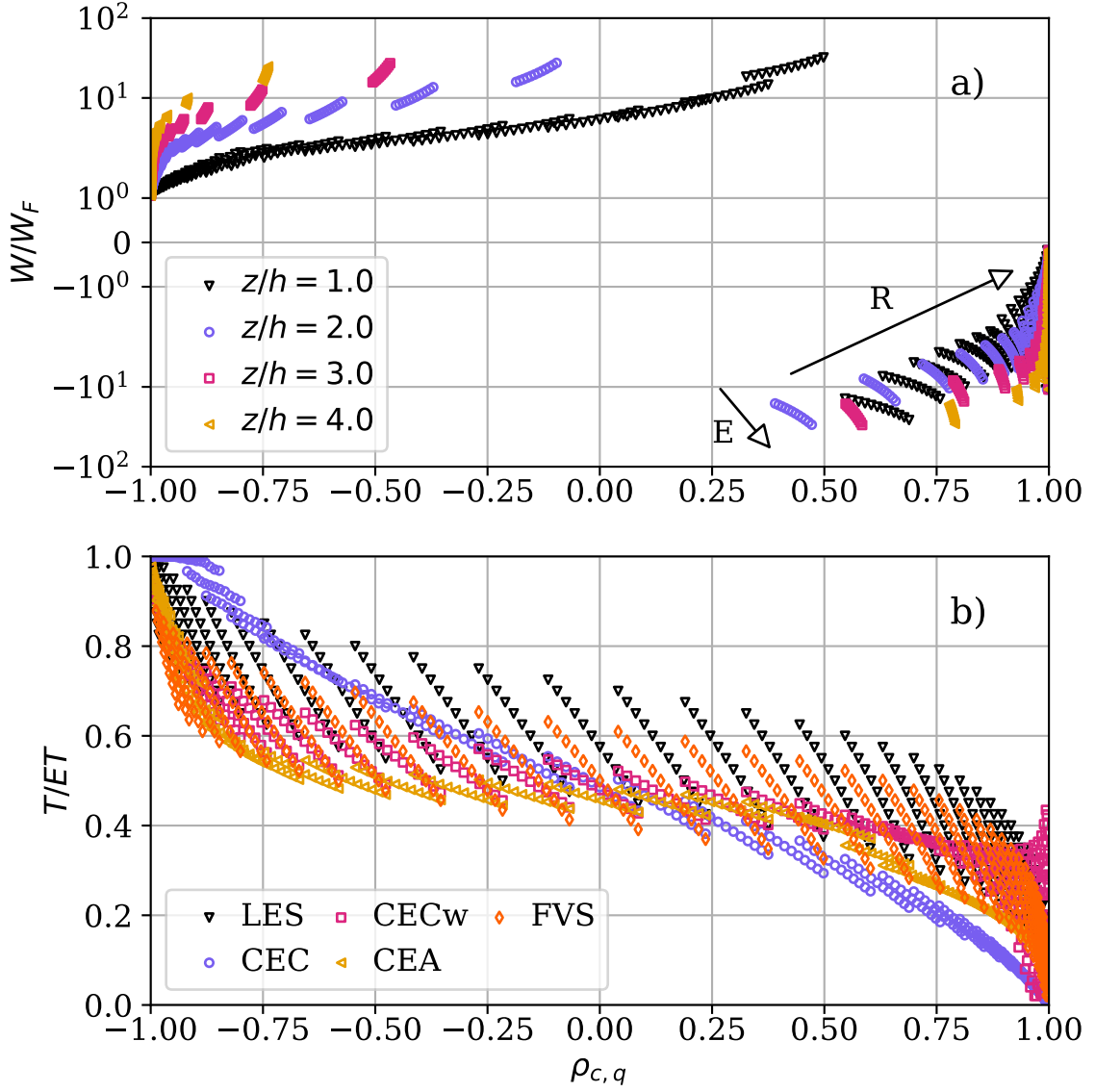


Figure 12. Panel (a) shows the relation between the ratio W/W_f and $\rho_{c,q}$ at heights $z/h = 1, 2, 3, 4$, where $W = P/T$ and $W_f = F_c/ET$ were computed from the imposed (“true”) flux components. Panel (b) shows the ratio T/ET versus correlation at $z/h = 1$ for the imposed (LES) values, as well as the results obtained by each partitioning method. A “cluster” of markers of the same color contains points with the same R/P ratio but different E/T ratios, and the different clusters thus have different R/P (as indicated by arrows of increasing R and E). Both panels contain only flux combinations following $-P/RP - 0.15 < T/ET < -P/RP + 0.15$ as shown in the delimited region in Figure 5.

(Zahn et al., 2022), which only used field data (although in that study the true flux components were not known).

As previously mentioned, the measurement or parameterization of the water-use efficiency in field experiments is still a challenge, and its connection to $\rho_{c,q}$ might help select the best parameterization model, or at least verify their plausibility, under certain

conditions. Therefore, the aim of the previous analysis in this section is to examine whether we can use $\rho_{c,q}$ as a screening tool for W/W_f , and ecosystem function more broadly. While such results cannot be generalized or be used for prediction with certainty at this point, they are a first good step towards obtaining more reliable ecosystem information from simple eddy-covariance measurements. To this end, we now replicate the analyses for water-use efficiency, as shown in Figure 12, using field data collected at the Treehaven forest (see Appendix B and table B1 for a description of the site). We calculate W from five different parametrizations of water use efficiency (all described in Zahn et al. (2022)), and then obtain the exact field-measured W_f and $\rho_{c,q}$. Figure 13 depicts W/W_f versus $\rho_{c,q}$ using these field data; we show the half-hourly data points as well as the average ratios (black markers) in bins of $\Delta\rho_{c,q} = 0.05$.

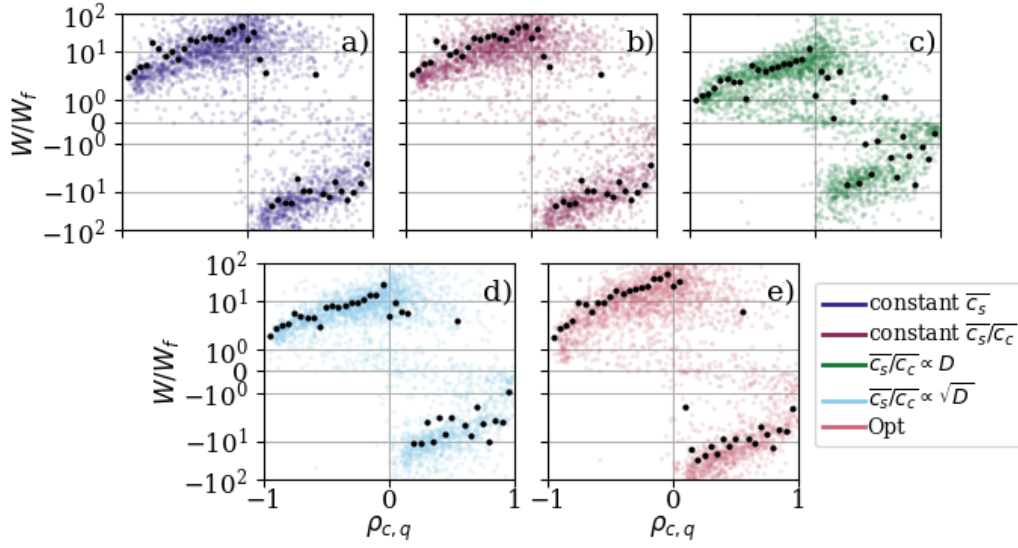


Figure 13. Scatter plot of the ratio W/W_f versus $\rho_{c,q}$ at the NEON site Treehaven (TREE), where $W_f = F_c/ET$. Black markers show the average over intervals $\Delta\rho_{c,q} = 0.05$. Data measured in Spring of 2018 and 2019, only for unstable conditions (*i.e.*, positive heat flux) and when W from all methods were available are shown. Each plot represents a different parameterization of the water-use efficiency, more specifically the parameterization of the interstomatal CO_2 concentration, \bar{c}_s . These models assume a) constant \bar{c}_s , b) constant ratio between interstomatal and near canopy CO_2 concentration, \bar{c}_s/\bar{c}_c , c) the ratio \bar{c}_s/\bar{c}_c is linearly proportional to vapor-pressure deficit (D), d) the ratio \bar{c}_s/\bar{c}_c is linearly proportional to \sqrt{D} , e) the optimization model proposed by (Scanlon et al., 2019). More details on each model are available in (Zahn et al., 2022).

Results for field data show a very similar trend (and magnitudes) to numerical results, where all models seem to follow a similar increase in the magnitude of W/W_f as the correlation tends towards zero (from either side). Furthermore, models involving the water-vapor pressure D (Figures c and d) seem less robust, showing more scatter and/or lower magnitudes of W/W_f than the remaining models. All models indicate a linear increase of W/W_f with increasingly positive correlation, which might suggest that these sites experience more variability in respiration than in evaporation (as can be inferred from the trends shown in figure 12). The same plot over three other NEON sites show similar results (Figures S14–S16 of the supplementary information). Overall, while this

analysis cannot evaluate the skill of a water-use efficiency model, it can increase our confidence in its use given that, on average, it follows the expected behavior with regards to $\rho_{c,q}$. In addition, filtering out data points that fall outside the two “clusters” that can be seen in figure 13 for positive and negative $\rho_{c,q}$ might help reducing periods with higher uncertainties.

5 Conclusion

In this study, we used large-eddy simulations to investigate partitioning methods that are based on the statistics of turbulent fluctuations of scalar concentrations above canopies. Our simulations replicated field experiments over homogeneous and heterogeneous (*i.e.*, with the presence of gaps in the vegetation) domains. The performance of each method — namely FVS, CEC, CEA, and CECw — were evaluated with regards to measurement height, flux component strength, and canopy structure. We can now synthesize the results to answer the five questions posed in the introduction.

1. The intercomparison of turbulent statistics across three different domains — a homogeneous forests, a “vineyard-like” canopy with parallel rows, and a domain with square “clusters” of vegetation — revealed how the presence of open gaps of exposed soil impacts partitioning methods. Overall, the larger these canyons (such as the cluster domain), the greater the mixing of scalars. As a consequence, mixing of q and c (from soil and canopy) occurs faster, and at lower heights, when large gaps are present in the domain. Thus, all partitioning methods were negatively impacted by increased canopy heterogeneity. This is the opposite of our initial hypothesis, which postulated that the presence of wider patches of soil would facilitate the separate sampling of ejections from the soil and from the canopy. Nonetheless, all methods still require a somewhat porous canopy to guarantee the coupling between the air masses above and below, and to allow ejections enriched in CO_2 to escape from the soil towards the sensor, as conceptualized by CEC, CEA and CECw methods. Therefore, homogeneous vegetation with a low to moderate LAI would be the best suited for these partitioning approaches.
2. Our numerical results indicate that CO_2 partitioning, almost invariably, had lower errors than evapotranspiration partitioning. The lowest errors occurred when the ratios T/E and P/R were proportional. Flux combinations where some methods performed poorly were usually characterized by atypical combinations, such as large photosynthesis but negligible transpiration, that are not expected in real field data. This lends confidence that these methods can provide results with sufficient accuracy to advance the understanding of ecosystems, optimize water use in agriculture, or for other practical applications where the carbon-water cycle coupling is important. Nonetheless, it is important to note that these “atypical” flux combinations might occur under specific circumstances. For instance, differences between anisohydric and isohydric stomatal behavior may manifest as differences that are perpendicular to the “ideal” diagonal. To this end, more research is needed to determine *a priori* when (and where) “off-diagonal” conditions are expected.
3. The best performance of CEC is expected near the canopy top ($z/h \approx 1$) when all flux components are non-negligible. CEA yielded comparable results to CEC, but outperformed the latter at all three levels in the context of numerical experiments. CECw also performed well at the canopy top, and its performance remained almost unaltered at higher levels. For a known water-use efficiency, the FVS method, followed by CECw, is the most reliable approach. Therefore, the choice of the best method to apply hinges on the measurement height, flux ratio, and uncertainty in W .
4. Partitioning estimates from FVS and CECw respond differently to over and underestimation of the water-use efficiency. By changing W by up to 100%, T_{FVS} changes by approximately $\pm 50\%$, while P_{FVS} can decrease by 100%. T_{CECw} , on

the other had, was found to be less sensitive to changes in W for the two cases investigated, while P_{CECw} increased/decreased by up to 100% as for the FVS method. Overall, these ranges can inform us about expected errors in the output of both methods as a result of uncertainties in W , which can vary significantly depending on the parameterization used.

5. By combining the CEC method and the water-use efficiency (CECw), we observed an improvement in the partitioning output relative to CEC. Not only does CECw result in smaller errors for a wider combination of flux components, but it also resulted in satisfactory accuracy at higher measurement elevations than CEC. This underscores the value of the information that the water-use efficiency adds to simple partitioning methods. In addition, given their shared connection through W , we suggest the concurrent implementation of FVS and CECw as a way to maximize the number of available solutions over a period.
6. Finally, we identified a connection between the water-use efficiency — a variable informing us about the plant functioning — and the correlation between q and c , a turbulent quantity. We further showed that this numerical result is in agreement with field data analyses. This exciting finding opens a path towards recovering biophysiological variables from simple high-frequency data measurements.
7. For readers interested in applying these methods for field data, and given the variability of the skill and solution availability of the different methods with measurement height, flux ratio, and input uncertainty, our recommendation is to concurrently apply all methods, and potentially MREA. This can increase confidence in the outputs when the methods agree, but when they do not, the various analyses presented here can guide the user on which method is most likely to be more accurate under given conditions. An important contribution in this regard of the present paper is the introduction of two new methods for this partitioning approach, the CECw and the CEA.

Because our analyses focused on neutral conditions, we cannot readily extrapolate these results to all stability conditions. Nonetheless, we hypothesize that as long as no strong stratification — hindering strong updrafts from carrying soil fluxes — or strong convection, strongly mixing the scalars — are present, the conclusions we draw in this paper should still be valid (*i.e.*, for weakly stable or unstable conditions). We also limited our exploration of canopy domain configuration to three cases; thus, it is possible that different results may emerge if, for instance, the gaps between rows of vegetation were smaller. Likewise, soil and canopy heterogeneity, including spatial variability of fluxes, LAI and LAD, would be closer to real canopies, but were out of the scope of the present study. Such additional analyses are left to future studies.

It is also important to acknowledge the inherent limitations of simulations in reproducing field experiments. For instance, given the resolution constraint, we are not able to represent all range of small eddies possibly carrying fluxes from surface and canopy and mixing the scalars, as well as the different scales of heterogeneity in real canopies. Likewise, simulations represent an idealized state (*e.g.*, neutral stability) rarely observed in field experiments. Thus, the results discussed in this paper depict a “baseline” scenario of how these methods operate, noting that these results may not hold exactly in field experiments for different reasons. For instance, a previous publication (Zahn et al., 2022) showed superior performance of CEC in partitioning transpiration above a grass site. Despite the superior numerical results obtained by CEA and FVS in the current paper, CEC still outperforms CEA and FVS above this site (Figure S17 in the supplementary information). To this end, additional implementation and comparison against independent measurements of one or more of flux components might help elucidate the performance of these methods in real ecosystems.

Overall, the results presented here contribute to better understanding of partitioning methods based on high-frequency eddy-covariance data. More importantly, they also

show the possibility of extracting valuable information from simple measurements that are becoming increasingly more available (eddy-covariance systems). Even when we take into account the specific site and/or meteorological conditions that meet the requirements for such analyses — thus reducing the number of ideal sites — we are still able to obtain new information across many potential sites at no cost of additional data. Furthermore, while these numerical findings should be applied with care to real measurements, our findings can guide the design of future experiments focusing on partitioning. To this end, the following considerations should be taken into account when designing new experiments: 1) the measurement height of the EC system should be as close to the canopy as possible ($z/h < 3$), ideally with one measurement level around $z/h \approx 1$ to better sample eddies emanating from the soil; 2) the canopy should be porous enough (visible soil from above), but ideally continuous (not patchy); 3) the partitioning methods should only be implemented (or trusted) when all four flux components are expected to be non-negligible.

Appendix A Validation of LES setup

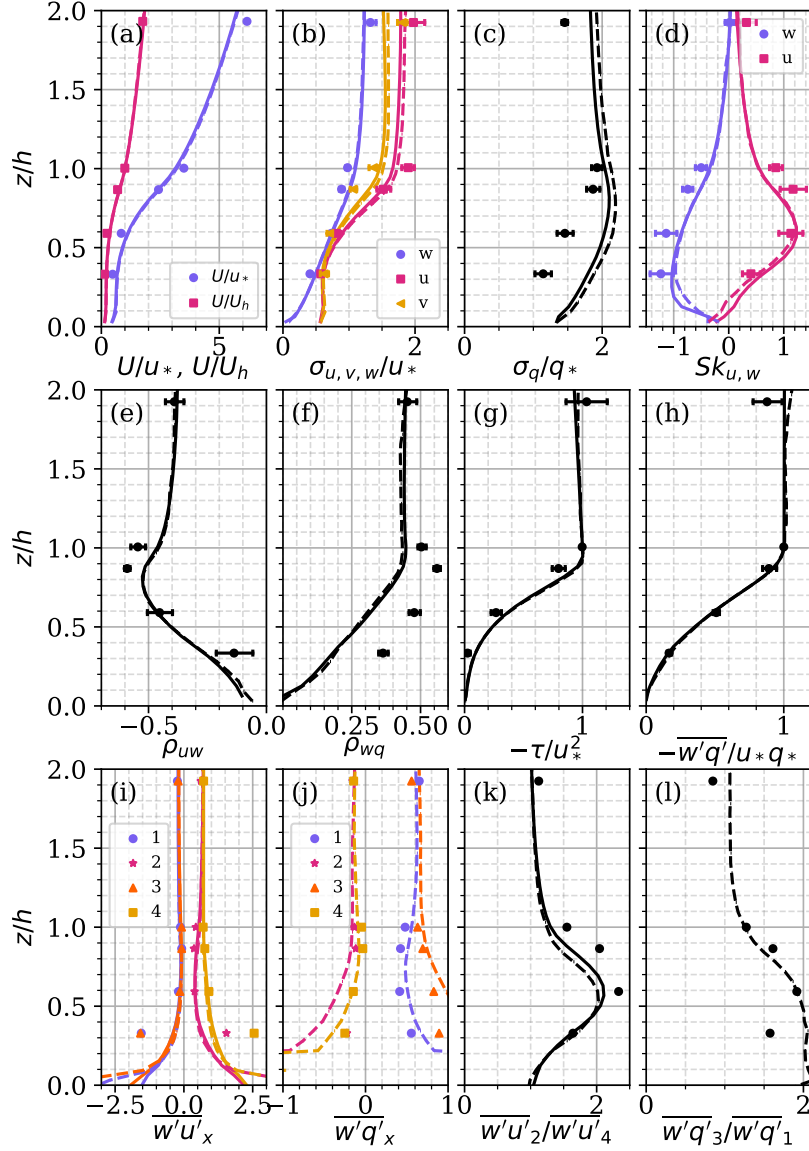


Figure A1. Validation of the LES set-up. Continuous lines represent the spatially and temporally averaged statistics, while dashed lines are the temporal statistics computed from the ensemble average of the 24 virtual eddy-covariance towers, and markers are statistics from a field experiment by (Shaw et al., 1988). Top row shows the velocity profile (a), nondimensional standard deviation of velocity components (b) and water vapor (c), and skewness of u and w (d). The middle row depicts the correlation coefficient between u and w (e) and w and q (f), and the nondimensional stress (g) and water vapor flux profiles (h). The bottom row shows the flux fraction in the four quadrants for momentum (i) and water vapor flux (j), while the ratio between quadrants is shown in (k) (sweeps/ejections) for momentum and (l) for water vapor fluxes.

Appendix B Experimental Data

High-frequency eddy-covariance data from four sites managed by the National Ecological Observatory Network (NEON) (2022) were downloaded for the years of 2018 and 2019. We selected these sites based on the low ratio between measurement (z) and canopy (h) heights. In addition, the forests are sparse enough such that some coupling between below and above canopy flows is expected. Thus, both the low measurement height and canopy sparseness satisfy the requirements for implementation of all partitioning methods, as discussed in Zahn et al. (2022). A brief description of each site is shown in Table B1.

Table B1. Summary of the experimental data used in this study. LAI is the leaf-area index (National Ecological Observatory Network, 2021) estimated by aerial images during summer.

Site ID	Name	Location	z/h	LAI
BONA	Bonanza Creek	Fairbanks North Star County, AK	2.4	1.8
DEJU	Delta Junction	Southeast Fairbanks County, AK	2.2	1.2
HARV	Harvard Forest	Worcester County, MA	1.5	1.9
TREE	Treehaven	Lincoln county, WI	1.6	-

Data were collected by the same instruments across all sites, consisting of an enclosed gas analyzer (model Li-7200, LiCor Inc., Lincoln, NB) and a three-dimensional sonic anemometer (model CSAT-3, Campbell Scientific Inc., Logan, UT) acquiring data at 20 Hz. The raw data were processed following the same procedures described in Zahn et al. (2022). In addition to computing turbulent quantities such as correlations and covariances, we also computed the water-use efficiency for these four sites as

$$W = 0.65 \frac{\overline{c_c} - \overline{c_s}}{\overline{q_c} - \overline{q_s}}, \quad (\text{B1})$$

where $\overline{q_c}$ and $\overline{c_c}$ are H_2O and CO_2 atmospheric mean concentrations near the canopy, and $\overline{q_s}$ and $\overline{c_s}$ are the mean intercellular concentrations. While $\overline{q_s}$ is calculated by assuming stomatal saturation, a parameterization needs to be adopted for $\overline{c_s}$. In our analysis, we implemented five different models for $\overline{c_s}$ described in Zahn et al. (2022), thus obtaining five estimates of W .

Appendix C Phase diagrams of sensitivity to water-use efficiency

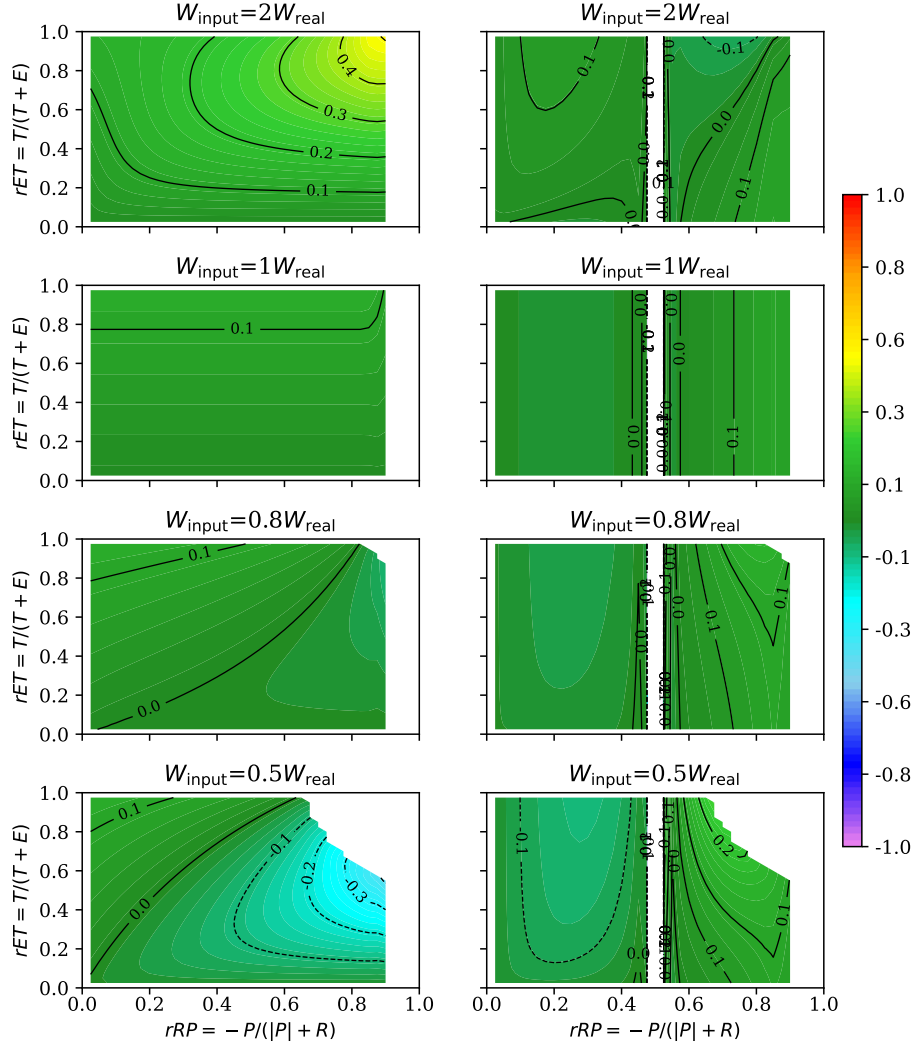


Figure C1. Phase diagrams indicating the sensitivity of the FVS method to uncertainties in the water-use efficiency. T_{FVS}/T is shown on the left side, while P_{FVS}/P is shown on the right side. Note that FVS does not find valid solutions when plant components dominate as W is underestimated.

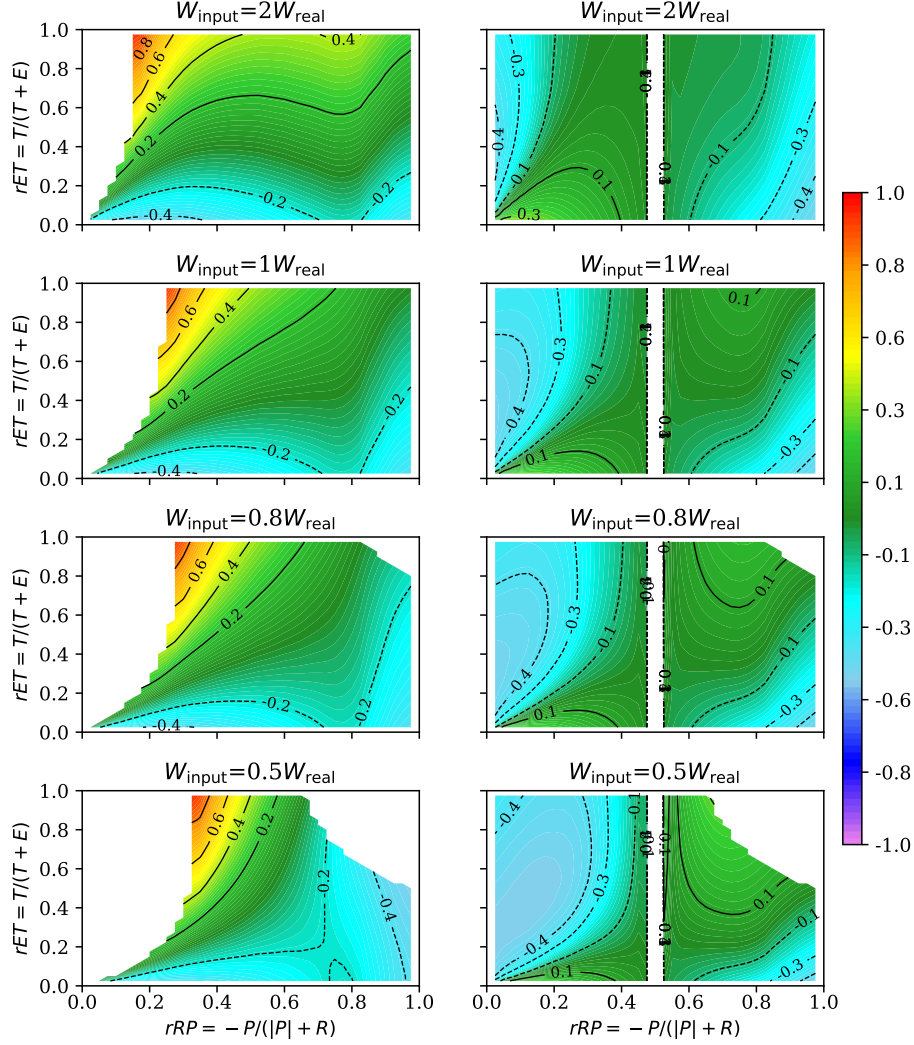


Figure C2. Phase diagrams indicating the sensitivity of the CECw method to uncertainties in the water-use efficiency. T_{CECw}/T is shown on the left side, while P_{CECw}/P is shown on the right side. Only errors of up to 100% ($T_{\text{CECw}}/T=2$ or $P_{\text{CECw}}/P=2$) are shown.

Open Research Section

The data and models of this paper will be openly shared upon acceptance, and the details to access them will be provided in this section

Acknowledgments

E.Z. and E.B.Z. are supported by the Moore Charitable Foundation Science-to-Action Fund from the School of Engineering and Applied Science at Princeton, and by the National Science Foundation under award EAR 2126206. We would like to acknowledge high-performance computing support from Cheyenne (Computational and Information Systems Laboratory, 2019) provided by NCAR's Computational and Information Systems Laboratory, sponsored by the National Science Foundation, under projects UPRI0007

and UPRI0021. S.P.G. is supported by the U.S. Department of Energy (Grant DE-SC0024297).
USDA is an equal opportunity provider and employer.

References

- Baslam, M., Mitsui, T., Hodges, M., Priesack, E., Herritt, M. T., Aranjuelo, I., & Sanz-Saez, A. (2020). Photosynthesis in a changing global climate: Scaling up and scaling down in crops. *Frontiers in Plant Science*, 11. Retrieved from <https://www.frontiersin.org/articles/10.3389/fpls.2020.00882> doi: 10.3389/fpls.2020.00882
- Bink, N. J., & Meesters, A. G. C. A. (1997). *Boundary-Layer Meteorology*, 84. doi: 10.1023/A:1000427431944
- Bou-Zeid, E., Meneveau, C., & Parlange, M. (2005). A scale-dependent lagrangian dynamic model for large eddy simulation of complex turbulent flows. *Physics of Fluids*, 17(2), 025105. Retrieved from <https://doi.org/10.1063/1.1839152> doi: 10.1063/1.1839152
- Businger, J. A., & Oncley, S. P. (1990). Flux measurement with conditional sampling. *Journal of Atmospheric and Oceanic Technology*, 7(2), 349-352. Retrieved from [https://doi.org/10.1175/1520-0426\(1990\)007<0349:FMWCS>2.0.CO;2](https://doi.org/10.1175/1520-0426(1990)007<0349:FMWCS>2.0.CO;2) doi: 10.1175/1520-0426(1990)007<0349:FMWCS>2.0.CO;2
- Chen, B., Chamecki, M., & Katul, G. G. (2020). Effects of gentle topography on forest-atmosphere gas exchanges and implications for eddy-covariance measurements. *Journal of Geophysical Research: Atmospheres*, 125(11), e2020JD032581. Retrieved from <https://agupubs.onlinelibrary.wiley.com/doi/abs/10.1029/2020JD032581> (e2020JD032581) doi: <https://doi.org/10.1029/2020JD032581>
- Computational and Information Systems Laboratory. (2019). *Cheyenne: HPE/SGI ICE XA System (University Community Computing)*. Boulder, CO: National Center for Atmospheric Research. doi: 10.5065/D6RX99HX
- Detto, M., & Katul, G. G. (2007). Simplified expressions for adjusting higher-order turbulent statistics obtained from open path gas analyzers. *Boundary-Layer Meteorology*, 122, 1573-1472. doi: 10.1007/s10546-006-9105-1
- Dupont, S., & Brunet, Y. (2008). Influence of foliar density profile on canopy flow: A large-eddy simulation study. *Agricultural and Forest Meteorology*, 148(6), 976-990. Retrieved from <https://www.sciencedirect.com/science/article/pii/S0168192308000336> doi: <https://doi.org/10.1016/j.agrformet.2008.01.014>
- Dusenage, M. E., Duarte, A. G., & Way, D. A. (2019). Plant carbon metabolism and climate change: elevated co2 and temperature impacts on photosynthesis, photorespiration and respiration. *New Phytologist*, 221(1), 32-49. Retrieved from <https://nph.onlinelibrary.wiley.com/doi/abs/10.1111/nph.15283> doi: <https://doi.org/10.1111/nph.15283>
- Edburg, S., Stock, D., Lamb, B., & Patton, E. (2012). The effect of the vertical source distribution on scalar statistics within and above a forest canopy. *Boundary-Layer Meteorology*, 142(3), 365 – 382. doi: 10.1007/s10546-011-9686-1
- Eichmann, E., Mantoani, M. C., Chamberlain, S. D., Hemes, K. S., Oikawa, P. Y., Szutu, D., ... Baldocchi, D. D. (2022). A novel approach to partitioning evapotranspiration into evaporation and transpiration in flooded ecosystems. *Global Change Biology*, 28(3), 990-1007. Retrieved from <https://onlinelibrary.wiley.com/doi/abs/10.1111/gcb.15974> doi: <https://doi.org/10.1111/gcb.15974>
- Fatichi, S., Paschalis, A., Bonetti, S., Manoli, G., & Pappas, C. (2022). Water use efficiency: A review of spatial and temporal variability. In *Reference module in earth systems and environmental sciences*. Elsevier. Retrieved from <https://>

- 1071 www.sciencedirect.com/science/article/pii/B978012822974300166X
 1072 doi: <https://doi.org/10.1016/B978-0-12-822974-3.00166-X>
- 1073 Gao, Z., Liu, H., Arntzen, E., McFarland, D. P., Chen, X., & Huang, M. (2020).
 1074 Uncertainties in turbulent statistics and fluxes of CO₂ associated with density
 1075 effect corrections. *Geophysical Research Letters*, 47(15), e2020GL088859.
 1076 Retrieved from [https://agupubs.onlinelibrary.wiley.com/doi/abs/](https://agupubs.onlinelibrary.wiley.com/doi/abs/10.1029/2020GL088859)
 1077 [10.1029/2020GL088859](https://doi.org/10.1029/2020GL088859) (e2020GL088859 2020GL088859) doi: [https://](https://doi.org/10.1029/2020GL088859)
 1078 doi.org/10.1029/2020GL088859
- 1079 Huang, J., & Bou-Zeid, E. (2013, 6). Turbulence and vertical fluxes in the stable
 1080 atmospheric boundary layer. part i: A large-eddy simulation study. *Journal of*
 1081 *the Atmospheric Sciences*, 70, 1513-1527. doi: 10.1175/JAS-D-12-0167.1
- 1082 Katul, G., Goltz, S. M., Hsieh, C.-I., Cheng, Y., Mowry, F., & Sigmon, J. (1995).
 1083 Estimation of surface heat and momentum fluxes using the flux-variance
 1084 method above uniform and non-uniform terrain. *Boundary-Layer Meteorology*, 74. Retrieved from <https://doi.org/10.1007/BF00712120> doi:
 1085 [10.1007/BF00712120](https://doi.org/10.1007/BF00712120)
 1086 [10.1007/BF00712120](https://doi.org/10.1007/BF00712120)
- 1087 Katul, G. G., Finkelstein, P. L., Clarke, J. F., & Ellestad, T. G. (1996). An inves-
 1088 tigation of the conditional sampling method used to estimate fluxes of active,
 1089 reactive, and passive scalars. *Journal of Applied Meteorology and Climatology*,
 1090 35(10), 1835-1845.
- 1091 Kirschbaum, M. U. F., & McMillan, A. M. S. (2018). Warming and elevated CO₂
 1092 have opposing influences on transpiration. which is more important? *Current*
 1093 *Forestry Reports*, 4, 51-71. doi: 10.1007/s40725-018-0073-8
- 1094 Klosterhalfen, A., Graf, A., Brüggemann, N., Drüe, C., Esser, O., González-Dugo,
 1095 M. P., ... Vereecken, H. (2019). Source partitioning of H₂O and CO₂
 1096 fluxes based on high-frequency eddy covariance data: a comparison between
 1097 study sites. *Biogeosciences*, 16(6), 1111-1132. Retrieved from [https://](https://www.biogeosciences.net/16/1111/2019/)
 1098 www.biogeosciences.net/16/1111/2019/ doi: 10.5194/bg-16-1111-2019
- 1099 Klosterhalfen, A., Moene, A., Schmidt, M., Scanlon, T., Vereecken, H., & Graf, A.
 1100 (2019). Sensitivity analysis of a source partitioning method for H₂O and CO₂
 1101 fluxes based on high frequency eddy covariance data: Findings from field data
 1102 and large eddy simulations. *Agricultural and Forest Meteorology*, 265, 152 -
 1103 170. Retrieved from [http://www.sciencedirect.com/science/article/pii/](http://www.sciencedirect.com/science/article/pii/S0168192318303496)
 1104 [S0168192318303496](http://www.sciencedirect.com/science/article/pii/S0168192318303496) doi: <https://doi.org/10.1016/j.agrformet.2018.11.003>
- 1105 Kumar, V., Kleissl, J., Meneveau, C., & Parlange, M. B. (2006). Large-eddy sim-
 1106 ulation of a diurnal cycle of the atmospheric boundary layer: Atmospheric
 1107 stability and scaling issues. *Water Resources Research*, 42(6). Retrieved
 1108 from [https://agupubs.onlinelibrary.wiley.com/doi/abs/10.1029/](https://agupubs.onlinelibrary.wiley.com/doi/abs/10.1029/2005WR004651)
 1109 [2005WR004651](https://doi.org/10.1029/2005WR004651) doi: <https://doi.org/10.1029/2005WR004651>
- 1110 Lasslop, G., Reichstein, M., Papale, D., Richardson, A. D., Arneth, A., Barr, A., ...
 1111 Wohlfahrt, G. (2010). Separation of net ecosystem exchange into assimilation
 1112 and respiration using a light response curve approach: critical issues and global
 1113 evaluation. *Global Change Biology*, 16(1), 187-208. Retrieved from [https://](https://onlinelibrary.wiley.com/doi/abs/10.1111/j.1365-2486.2009.02041.x)
 1114 onlinelibrary.wiley.com/doi/abs/10.1111/j.1365-2486.2009.02041.x
 1115 doi: <https://doi.org/10.1111/j.1365-2486.2009.02041.x>
- 1116 Li, Q., & Bou-Zeid, E. (2019). Contrasts between momentum and scalar transport
 1117 over very rough surfaces. *Journal of Fluid Mechanics*, 880, 32-58. doi: 10
 1118 .1017/jfm.2019.687
- 1119 Li, X., Gentine, P., Lin, C., Zhou, S., Sun, Z., Zheng, Y., ... Zheng, C. (2019). A
 1120 simple and objective method to partition evapotranspiration into transpiration
 1121 and evaporation at eddy-covariance sites. *Agricultural and Forest Meteorology*, 265, 171 - 182. Retrieved from [http://www.sciencedirect.com/](http://www.sciencedirect.com/science/article/pii/S016819231830371X)
 1122 [science/article/pii/S016819231830371X](http://www.sciencedirect.com/science/article/pii/S016819231830371X) doi: [https://doi.org/10.1016/](https://doi.org/10.1016/j.agrformet.2018.11.017)
 1123 [j.agrformet.2018.11.017](https://doi.org/10.1016/j.agrformet.2018.11.017)
 1124 [j.agrformet.2018.11.017](https://doi.org/10.1016/j.agrformet.2018.11.017)

- 1125 Mao, S., Leclerc, M. Y., & Michaelides, E. E. (2008). Passive scalar flux foot-
 1126 print analysis over horizontally inhomogeneous plant canopy using large-
 1127 eddy simulation. *Atmospheric Environment*, 42(21), 5446-5458. Re-
 1128 trieved from [https://www.sciencedirect.com/science/article/pii/](https://www.sciencedirect.com/science/article/pii/S1352231008001908)
 1129 [S1352231008001908](https://www.sciencedirect.com/science/article/pii/S1352231008001908) doi: <https://doi.org/10.1016/j.atmosenv.2008.02.029>
- 1130 Mengis, N., Keller, D. P., Eby, M., & Oschlies, A. (2015, aug). Uncertainty in the
 1131 response of transpiration to co2 and implications for climate change. *Environ-*
 1132 *mental Research Letters*, 10(9), 094001. Retrieved from [https://dx.doi.org/](https://dx.doi.org/10.1088/1748-9326/10/9/094001)
 1133 [10.1088/1748-9326/10/9/094001](https://dx.doi.org/10.1088/1748-9326/10/9/094001) doi: 10.1088/1748-9326/10/9/094001
- 1134 National Ecological Observatory Network. (2021). *LAI - spectrome-*
 1135 *ter - flightline (dp2.30012.001)*. [https://data.neonscience.org/data-](https://data.neonscience.org/data-products/DP2.30012.001/RELEASE-2021)
 1136 [products/DP2.30012.001/RELEASE-2021](https://data.neonscience.org/data-products/DP2.30012.001/RELEASE-2021). National Ecological Observatory
 1137 Network (NEON). doi: 10.48443/ABRM-BS86
- 1138 National Ecological Observatory Network (NEON). (2022). *Bundled data products*
 1139 *- eddy covariance (dp4.00200.001)*. National Ecological Observatory Network
 1140 (NEON). Retrieved from [https://data.neonscience.org/data-products/](https://data.neonscience.org/data-products/DP4.00200.001/RELEASE-2022)
 1141 [DP4.00200.001/RELEASE-2022](https://data.neonscience.org/data-products/DP4.00200.001/RELEASE-2022) doi: 10.48443/7CQP-3J73
- 1142 Nelson, J. A., Carvalhais, N., Cuntz, M., Delpierre, N., Knauer, J., Ogée, J., ...
 1143 Jung, M. (2018). Coupling water and carbon fluxes to constrain esti-
 1144 mates of transpiration: The tea algorithm. *Journal of Geophysical Re-*
 1145 *search: Biogeosciences*, 123(12), 3617-3632. Retrieved from [https://](https://agupubs.onlinelibrary.wiley.com/doi/abs/10.1029/2018JG004727)
 1146 agupubs.onlinelibrary.wiley.com/doi/abs/10.1029/2018JG004727 doi:
 1147 [10.1029/2018JG004727](https://doi.org/10.1029/2018JG004727)
- 1148 Nelson, J. A., Pérez-Priego, O., Zhou, S., Poyatos, R., Zhang, Y., Blanken, P. D., ...
 1149 Jung, M. (2020). Ecosystem transpiration and evaporation: Insights from three
 1150 water flux partitioning methods across fluxnet sites. *Global Change Biology*,
 1151 *n/a(n/a)*. Retrieved from [https://onlinelibrary.wiley.com/doi/abs/](https://onlinelibrary.wiley.com/doi/abs/10.1111/gcb.15314)
 1152 [10.1111/gcb.15314](https://onlinelibrary.wiley.com/doi/abs/10.1111/gcb.15314) doi: 10.1111/gcb.15314
- 1153 Pan, Y., Chamecki, M., & Isard, S. A. (2014). Large-eddy simulation of turbulence
 1154 and particle dispersion inside the canopy roughness sublayer. *Journal of Fluid*
 1155 *Mechanics*, 753, 499-534. doi: 10.1017/jfm.2014.379
- 1156 Pan, Y., Follett, E., Chamecki, M., & Nepf, H. (2014). Strong and weak, unsteady
 1157 reconfiguration and its impact on turbulence structure within plant canopies.
 1158 *Physics of Fluids*, 26(10), 105102. Retrieved from [https://doi.org/10.1063/](https://doi.org/10.1063/1.4898395)
 1159 [1.4898395](https://doi.org/10.1063/1.4898395) doi: 10.1063/1.4898395
- 1160 Pattey, E., Edwards, G., Strachan, I. B., Desjardins, R. L., Kaharabata, S., & Wag-
 1161 ner Riddle, C. (2006). Towards standards for measuring greenhouse gas fluxes
 1162 from agricultural fields using instrumented towers. *Canadian Journal of Soil*
 1163 *Science*, 86(3), 373-400. Retrieved from <https://doi.org/10.4141/S05-100>
 1164 [doi: 10.4141/S05-100](https://doi.org/10.4141/S05-100)
- 1165 Perez-Priego, O., Katul, G., Reichstein, M., El-Madany, T. S., Ahrens, B., Carrara,
 1166 A., ... Migliavacca, M. (2018). Partitioning eddy covariance water flux com-
 1167 ponents using physiological and micrometeorological approaches. *Journal*
 1168 *of Geophysical Research: Biogeosciences*, 123(10), 3353-3370. Retrieved
 1169 from [https://agupubs.onlinelibrary.wiley.com/doi/abs/10.1029/](https://agupubs.onlinelibrary.wiley.com/doi/abs/10.1029/2018JG004637)
 1170 [2018JG004637](https://agupubs.onlinelibrary.wiley.com/doi/abs/10.1029/2018JG004637) doi: 10.1029/2018JG004637
- 1171 Reichstein, M., Falge, E., Baldocchi, D., Papale, D., Aubinet, M., Berbigier, P.,
 1172 ... Valentini, R. (2005). On the separation of net ecosystem exchange
 1173 into assimilation and ecosystem respiration: review and improved algo-
 1174 rithm. *Global Change Biology*, 11(9), 1424-1439. Retrieved from [https://](https://onlinelibrary.wiley.com/doi/abs/10.1111/j.1365-2486.2005.001002.x)
 1175 onlinelibrary.wiley.com/doi/abs/10.1111/j.1365-2486.2005.001002.x
 1176 doi: <https://doi.org/10.1111/j.1365-2486.2005.001002.x>
- 1177 Rigden, A. J., Salvucci, G. D., Entekhabi, D., & Short Gianotti, D. J. (2018). Par-
 1178 titioning evapotranspiration over the continental united states using weather
 1179 station data. *Geophysical Research Letters*, 45(18), 9605-9613. Retrieved

- from <https://agupubs.onlinelibrary.wiley.com/doi/abs/10.1029/2018GL079121> doi: <https://doi.org/10.1029/2018GL079121>
- Scanlon, T. M., & Kustas, W. P. (2010). Partitioning carbon dioxide and water vapor fluxes using correlation analysis. *Agricultural and Forest Meteorology*, 150(1), 89 - 99. Retrieved from <http://www.sciencedirect.com/science/article/pii/S0168192309002214> doi: <https://doi.org/10.1016/j.agrformet.2009.09.005>
- Scanlon, T. M., & Sahu, P. (2008). On the correlation structure of water vapor and carbon dioxide in the atmospheric surface layer: A basis for flux partitioning. *Water Resources Research*, 44(10). Retrieved from <https://agupubs.onlinelibrary.wiley.com/doi/abs/10.1029/2008WR006932> doi: 10.1029/2008WR006932
- Scanlon, T. M., Schmidt, D. F., & Skaggs, T. H. (2019). Correlation-based flux partitioning of water vapor and carbon dioxide fluxes: Method simplification and estimation of canopy water use efficiency. *Agricultural and Forest Meteorology*, 279, 107732. Retrieved from <http://www.sciencedirect.com/science/article/pii/S016819231930348X> doi: <https://doi.org/10.1016/j.agrformet.2019.107732>
- Scott, R. L., & Biederman, J. A. (2017). Partitioning evapotranspiration using long-term carbon dioxide and water vapor fluxes. *Geophysical Research Letters*, 44(13), 6833-6840. Retrieved from <https://agupubs.onlinelibrary.wiley.com/doi/abs/10.1002/2017GL074324> doi: 10.1002/2017GL074324
- Shaw, R. H., Den Hartog, G., & Neumann, H. H. (1988). Influence of foliar density and thermal stability on profiles of reynolds stress and turbulence intensity in a deciduous forest. *Boundary-Layer Meteorology*, 45. doi: 10.1007/BF00124010
- Shaw, R. H., & Schumann, U. (1992). Large-eddy simulation of turbulent flow above and within a forest. *Boundary-Layer Meteorology*, 61. doi: 10.1007/BF02033994
- Skaggs, T., Anderson, R., Alfieri, J., Scanlon, T., & Kustas, W. (2018). Fluxpart: Open source software for partitioning carbon dioxide and water vapor fluxes. *Agricultural and Forest Meteorology*, 253-254, 218 - 224. Retrieved from <http://www.sciencedirect.com/science/article/pii/S0168192318300698> doi: <https://doi.org/10.1016/j.agrformet.2018.02.019>
- Stoll, R., Gibbs, J. A., Salesky, S. T., Anderson, W., & Calaf, M. (2020, August). Large-eddy simulation of the atmospheric boundary layer. *Boundary-Layer Meteorology*, 177(2-3), 541-581. Retrieved from <http://dx.doi.org/10.1007/s10546-020-00556-3> doi: 10.1007/s10546-020-00556-3
- Su, H.-B., Shaw, R. H., Paw, K. T., Moeng, C.-H., & Sullivan, P. P. (1998). Turbulent statistics of neutrally stratified flow within and above a sparse forest from large-eddy simulation and field observations. *Boundary-Layer Meteorology*, 88. doi: 10.1023/A:1001108411184
- Sulman, B. N., Roman, D. T., Scanlon, T. M., Wang, L., & Novick, K. A. (2016). Comparing methods for partitioning a decade of carbon dioxide and water vapor fluxes in a temperate forest. *Agricultural and Forest Meteorology*, 226-227, 229 - 245. Retrieved from <http://www.sciencedirect.com/science/article/pii/S0168192316302994> doi: <https://doi.org/10.1016/j.agrformet.2016.06.002>
- Thomas, C., Martin, J., Goeckede, M., Siqueira, M., Foken, T., Law, B., ... Katul, G. (2008). Estimating daytime subcanopy respiration from conditional sampling methods applied to multi-scalar high frequency turbulence time series. *Agricultural and Forest Meteorology*, 148(8), 1210 - 1229. Retrieved from <http://www.sciencedirect.com/science/article/pii/S0168192308000737> doi: <https://doi.org/10.1016/j.agrformet.2008.03.002>

- Thomas, C. K., Martin, J. G., Law, B. E., & Davis, K. (2013). Toward biologically meaningful net carbon exchange estimates for tall, dense canopies: Multi-level eddy covariance observations and canopy coupling regimes in a mature douglas-fir forest in oregon. *Agricultural and Forest Meteorology*, 173, 14 - 27. Retrieved from <http://www.sciencedirect.com/science/article/pii/S0168192313000051> doi: <https://doi.org/10.1016/j.agrformet.2013.01.001>
- Wagle, P., Skaggs, T. H., Gowda, P. H., Northup, B. K., & Neel, J. P. (2020). Flux variance similarity-based partitioning of evapotranspiration over a rainfed alfalfa field using high frequency eddy covariance data. *Agricultural and Forest Meteorology*, 285-286, 107907. Retrieved from <http://www.sciencedirect.com/science/article/pii/S0168192320300095> doi: <https://doi.org/10.1016/j.agrformet.2020.107907>
- Wagle, P., Skaggs, T. H., Gowda, P. H., Northup, B. K., Neel, J. P. S., & Anderson, R. G. (2021). Evaluation of water use efficiency algorithms for flux variance similarity-based evapotranspiration partitioning in c3 and c4 grain crops. *Water Resources Research*, 57(5), e2020WR028866. Retrieved from <https://agupubs.onlinelibrary.wiley.com/doi/abs/10.1029/2020WR028866> doi: <https://doi.org/10.1029/2020WR028866>
- Wang, K., Bastos, A., Ciais, P., Wang, X., Rodenbeck, C., Gentine, P., ... Piao, S. (2022). Regional and seasonal partitioning of water and temperature controls on global land carbon uptake variability. *Nature Communications*, 13. Retrieved from <https://doi.org/10.1038/s41467-022-31175-w> doi: [10.1038/s41467-022-31175-w](https://doi.org/10.1038/s41467-022-31175-w)
- Watanabe, T. (2004). Large-eddy simulation of coherent turbulence structures associated with scalar ramps over plant canopies. *Boundary-Layer Meteorology*, 112, 307-341. doi: <https://doi.org/10.1023/B:BOUN.0000027912.84492.54>
- Wei, Z., Yoshimura, K., Wang, L., Miralles, D. G., Jasechko, S., & Lee, X. (2017). Revisiting the contribution of transpiration to global terrestrial evapotranspiration. *Geophysical Research Letters*, 44(6), 2792-2801. Retrieved from <https://agupubs.onlinelibrary.wiley.com/doi/abs/10.1002/2016GL072235> doi: [10.1002/2016GL072235](https://doi.org/10.1002/2016GL072235)
- Xu, L., Baldocchi, D. D., & Tang, J. (2004). How soil moisture, rain pulses, and growth alter the response of ecosystem respiration to temperature. *Global Biogeochemical Cycles*, 18(4). Retrieved from <https://agupubs.onlinelibrary.wiley.com/doi/abs/10.1029/2004GB002281> doi: <https://doi.org/10.1029/2004GB002281>
- Yue, W., Parlange, M. B., Meneveau, C., Zhu, W., van Hout, R., & Katz, J. (2007). Large-eddy simulation of plant canopy flows using plant-scale representation. *Boundary-Layer Meteorology*, 124. doi: [10.1007/s10546-007-9173-x](https://doi.org/10.1007/s10546-007-9173-x)
- Zahn, E., & Bou-Zeid, E. (2023). Setting up a large-eddy simulation to focus on the atmospheric surface layer. *Boundary-Layer Meteorology*. Retrieved from <https://doi.org/10.1007/s10546-023-00841-x> doi: [10.1007/s10546-023-00841-x](https://doi.org/10.1007/s10546-023-00841-x)
- Zahn, E., Bou-Zeid, E., & Dias, N. L. (2023). Relaxed eddy accumulation outperforms monin-obukhov flux models under non-ideal conditions. *Geophysical Research Letters*, 50(7), e2023GL103099. Retrieved from <https://agupubs.onlinelibrary.wiley.com/doi/abs/10.1029/2023GL103099> (e2023GL103099 2023GL103099) doi: <https://doi.org/10.1029/2023GL103099>
- Zahn, E., Bou-Zeid, E., Good, S. P., Katul, G. G., Thomas, C. K., Ghannam, K., ... Kustas, W. P. (2022). Direct partitioning of eddy-covariance water and carbon dioxide fluxes into ground and plant components. *Agricultural and Forest Meteorology*, 315, 108790. Retrieved from <https://www.sciencedirect.com/science/article/pii/S0168192321004767> doi: <https://doi.org/10.1016/j.agrformet.2021.108790>

1288 Zhou, S., Yu, B., Zhang, Y., Huang, Y., & Wang, G. (2016). Partitioning evap-
1289 otranspiration based on the concept of underlying water use efficiency.
1290 *Water Resources Research*, 52(2), 1160-1175. Retrieved from [https://](https://agupubs.onlinelibrary.wiley.com/doi/abs/10.1002/2015WR017766)
1291 agupubs.onlinelibrary.wiley.com/doi/abs/10.1002/2015WR017766 doi:
1292 10.1002/2015WR017766